Weierstraß-Institut

für Angewandte Analysis und Stochastik

Leibniz-Institut im Forschungsverbund Berlin e. V.

On iterative subdomain methods for the Stokes–Darcy problem

Alfonso Caiazzo[1], Volker John[1,2] , Ulrich Wilbrandt[2]

submitted: July 10, 2013

[1] Weierstrass Institute
    Mohrenstr. 39
    10117 Berlin
    Germany
    email: Alfonso.Caiazzo@wias-berlin.de
            Volker.John@wias-berlin.de

[2] Free University of Berlin
    Department of Mathematics and Computer Science
    Arnimallee 6
    14195 Berlin, Germany
    email: uli-wilbrandt@gmx.de

No. 1812

Berlin 2013

Abstract

Iterative subdomain methods for the Stokes–Darcy problem that use Robin boundary conditions on the interface are reviewed. Their common underlying structure and their main differences are identified. In particular, it is clarified that there are different updating strategies for the interface conditions. For small values of fluid viscosity and hydraulic permeability, which are relevant in applications from geosciences, it is shown in numerical studies that only one of these updating strategies leads to an efficient numerical method, if this strategy is used in combination with appropriate parameters in the Robin boundary conditions. In particular, it is observed that the values of appropriate parameters are larger than those proposed so far. Not only the size but also the ratio of appropriate Robin parameters depends on the coefficients of the problem.

1. INTRODUCTION

Let us consider a bounded domain $\Omega \subset \mathbb{R}^d$, $d \in \{2, 3\}$, and a decomposition

$$\Omega = \Omega_{\mathrm{f}} \cup \Gamma_{\mathrm{I}} \cup \Omega_{\mathrm{p}} \,,$$

into two disjoint subdomains Ω_{f} and Ω_{p}, denoting a free flow domain and a porous medium, respectively, and possessing a common interface Γ_{I}, i.e., $\Omega_{\mathrm{f}} \cap \Omega_{\mathrm{p}} = \emptyset$ and $\overline{\Omega_{\mathrm{f}}} \cap \overline{\Omega_{\mathrm{p}}} = \Gamma_{\mathrm{I}}$, see Figure 1.

Assuming a moderate flow velocity in the free flow domain, the fluid dynamics in Ω_{f} can be modeled with the incompressible Stokes equations for the velocity $\mathbf{u}_{\mathrm{f}} \;:\; \Omega_{\mathrm{f}} \to \mathbb{R}^d \; [m/s]$ and the pressure $P_{\mathrm{f}} \;:\; \Omega_{\mathrm{f}} \to \mathbb{R} \; [Pa]$

$$-\nabla \cdot \mathbb{T}\left(\mathbf{u}_{\mathrm{f}}, \frac{P_{\mathrm{f}}}{\rho}\right) = \mathbf{f}_{\mathrm{f}} \text{ in } \Omega_{\mathrm{f}}, \tag{1}$$

$$\nabla \cdot \mathbf{u}_{\mathrm{f}} = 0 \text{ in } \Omega_{\mathrm{f}}. \tag{2}$$

In (1), $\rho \; [kg/m^3]$ represents the fluid density and $\mathbb{T}(\mathbf{u}_{\mathrm{f}}, p_{\mathrm{f}}) \; [m^2/s^2]$ denotes the fluid stress tensor

$$\mathbb{T}(\mathbf{u}_{\mathrm{f}}, p_{\mathrm{f}}) \;:\; \Omega_{\mathrm{f}} \to \mathbb{R}^{d \times d}, \quad \mathbb{T} = 2\nu \mathbb{D}(\mathbf{u}_{\mathrm{f}}) - p_{\mathrm{f}}\mathbb{I},$$
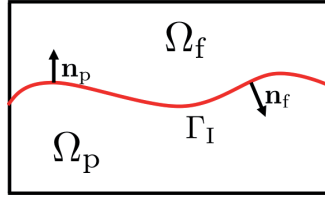
Figure 1. Sketch of the fluid domain for the Stokes–Darcy problems.

where $\mathbb{D}(\mathbf{u}_\mathrm{f}) = (\nabla \mathbf{u} + \nabla \mathbf{u}^T)/2$: $\Omega_\mathrm{f} \to \mathbb{R}^{d \times d}$ $[1/s]$ is the velocity deformation tensor, $p_\mathrm{f} = P_\mathrm{f}/\rho$ $[m^2/s^2]$, and ν : $\Omega_\mathrm{f} \to \mathbb{R}$ $[m^2/s]$ denotes the kinematic viscosity of the fluid. Outer forces acting on the free flow are modeled by $\mathbf{f}_\mathrm{f}$: $\Omega_\mathrm{f} \to \mathbb{R}^d$ $[m/s^2]$.

The dynamics in the porous medium is described by the Darcy law

$$\mathbb{K}\nabla\varphi_\mathrm{p} + \mathbf{u}_\mathrm{p} = \mathbf{0} \quad \text{in } \Omega_\mathrm{p}, \tag{3}$$

$$\nabla \cdot \mathbf{u}_\mathrm{p} = f_\mathrm{p} \text{ in } \Omega_\mathrm{p}, \tag{4}$$

in terms of the function φ_p : $\Omega_\mathrm{p} \to \mathbb{R}$ $[m]$, called Darcy pressure or piezometric head, and of the Darcy velocity $\mathbf{u}_\mathrm{p}$: $\Omega_\mathrm{p} \to \mathbb{R}^d$ $[m/s]$. In (3), $\mathbb{K}$: $\Omega_\mathrm{p} \to \mathbb{R}^{d \times d}$ $[m/s]$ is the hydraulic conductivity tensor. Generally, it will be assumed that $\mathbb{K} = \mathbb{K}^T$, $\mathbb{K} > 0$. Here, only the case $\mathbb{K} = K\mathbb{I}$, $K > 0$, will be considered. In (4), the function f_p : $\Omega_\mathrm{p} \to \mathbb{R}$ $[1/s]$ describes sinks and sources.

System (3)–(4) is called the mixed form of the Darcy problem. An alternative formulation is obtained by taking the divergence of equation (3) and using (4),

$$-\nabla \cdot (\mathbb{K}\nabla\varphi_\mathrm{p}) = f_\mathrm{p} \text{ in } \Omega_\mathrm{p}, \tag{5}$$

which is referred to as the primal form of the Darcy problem.

The mixed form is often more important for applications, as it allows to recover the Darcy velocity $\mathbf{u}_\mathrm{p}$ directly as an unknown of the problem. However, in what follows, we will focus on the primal formulation, which is generally simpler from the analytical and numerical point of view. Having computed φ_p with the primal formulation, the velocity $\mathbf{u}_\mathrm{p}$ can be computed in a post-processing step using (3). In the context of finite element methods, the application of (3) results in loosing one approximation order such that the approximation estimate for $\mathbf{u}_\mathrm{p}$ is worse than for φ_p. On the other hand, velocity post-processing techniques based on gradient super convergence phenomena have been successfully used to enforce mass conservation and improve global accuracy, see, e.g., [1]. Our motivation for considering the primal formulation lies in the fact that for the studied numerical methods there are already open questions for this formulation. These questions should be studied before proceeding to the more complicated mixed formulation.

Equations (1), (2), and (5) must be completed with appropriate boundary conditions and in particular with proper interface conditions at the Stokes–Darcy interface Γ_I. Denote by $\mathbf{n}_\mathrm{f}$ and $\mathbf{n}_\mathrm{p}$ the unit outward normal vectors on $\partial\Omega_\mathrm{f}$ and $\partial\Omega_\mathrm{p}$, respectively, and by $\boldsymbol{\tau}_i, i = 1, \ldots, d-1$, pairwise orthogonal unit tangential vectors on the interface Γ_I. Note that $\mathbf{n}_\mathrm{f} = -\mathbf{n}_\mathrm{p}$ on Γ_I. Two standard coupling conditions on Γ_I model the conservation of mass and the balance of normal stresses

$$\mathbf{u}_\mathrm{f} \cdot \mathbf{n}_\mathrm{f} = -\mathbb{K}\nabla\varphi_\mathrm{p} \cdot \mathbf{n}_\mathrm{f} \text{ on } \Gamma_\mathrm{I}, \tag{6}$$

$$-\mathbf{n}_\mathrm{f} \cdot \mathbb{T}(\mathbf{u}_\mathrm{f}, p_\mathrm{f}) \cdot \mathbf{n}_\mathrm{f} = g\varphi_\mathrm{p} \qquad \text{on } \Gamma_\mathrm{I}, \tag{7}$$

where g $[m/s^2]$ is the gravitational acceleration. A classical third coupling condition is the so-called Beavers–Joseph condition [2], which is based on experimental findings relating the jump of the tangential velocity along the interface to the fluid stresses:

$$(\mathbf{u}_\mathrm{f} - \mathbf{u}_\mathrm{p}) \cdot \boldsymbol{\tau}_i + \alpha\boldsymbol{\tau}_i \cdot \mathbb{T}(\mathbf{u}_\mathrm{f}, p_\mathrm{f}) \cdot \mathbf{n}_\mathrm{f} = 0 \text{ on } \Gamma_\mathrm{I}, i = 1, \ldots, d-1, \tag{8}$$

where

$$\alpha = \alpha_0 \sqrt{\frac{\boldsymbol{\tau}_i \cdot \mathbb{K} \cdot \boldsymbol{\tau}_i}{\nu g}} \ [s/m],$$

and $\alpha_0 > 0$ is a non-dimensional parameter depending on the properties of the porous medium, which must be experimentally determined. The well-posedness of the Beavers–Joseph interface condition (8) for the steady-state Stokes–Darcy problem is established only for particular values of α_0, see, e.g., [3, 4, 5]. Based on the observation that the Darcy velocity on Γ_I is often negligible compared with the Stokes velocity, it was proposed [6, 7] to simplify (8) to

$$\mathbf{u}_f \cdot \boldsymbol{\tau}_i + \alpha \boldsymbol{\tau}_i \cdot \mathbb{T}(\mathbf{u}_f, p_f) \cdot \mathbf{n}_f = 0 \quad \text{on } \Gamma_I, i = 1, \ldots, d-1, \tag{9}$$

which is called Beavers–Joseph–Saffman condition (or Beavers–Joseph–Saffman–Jones condition). A further simplification is based on the observation that both terms on the left-hand side of (9) are small, hence obtaining

$$\mathbf{u}_f \cdot \boldsymbol{\tau}_i = 0 \quad \text{on } \Gamma_I, i = 1, \ldots, d-1. \tag{10}$$

The coupled problem defined by (1), (2), (5) with the conditions (6), (7), and (9) (or (10)) has been studied extensively in the literature both theoretically, see, among others, [3, 5, 8, 9], and numerically, e.g., [4, 10, 11, 12, 13, 14, 15, 16, 17]. This report will consider the interface conditions (9) and (10) and different numerical methods to solve the resulting coupled problems in a finite element framework. Since (9) and (10) do not couple the Stokes and the Darcy equations, they yield formulations simpler to analyze and to treat numerically than (8), see, e.g., [10, 16]. Nonetheless, several questions are still open.

The numerical methods for solving the coupled problem might be divided into two main classes. Direct (also called monolithic or single domain) methods aim at solving in a single step the whole coupled system. Proposals of finite element based approaches to solve the strongly coupled Stokes–Darcy problem can be found, among others, in [18, 19, 20, 21, 22, 23, 13]. These techniques are in general stable and robust. However, they might be computationally costly, depending on the size of the problem and on the physics behind it. Preconditioned direct methods based on solving the problems on different grids are proposed in [24, 25]. As an alternative, decoupled (also called domain-decomposition or multidomain) approaches solve the coupled problem with a subdomain iterative procedure based, at each iteration, on the solution of the Stokes and Darcy problem separately. On the one hand, an iterative method requires multiple solutions of the subproblems. On the other hand, the advantage of these techniques is that they allow to use specialized solvers for Stokes and Darcy problems and to tailor the algorithms according to their mathematical and physical properties, which might result in efficient procedures. Furthermore, iterative approaches are generally preferred if efficient solvers for the subproblems are available. Our motivation for studying the coupled Stokes–Darcy problem comes from the numerical simulation of the fluid dynamics in water basins and river beds. The discretization of these problems is characterized by complex geometries and might lead to large and ill-conditioned systems in three dimensions. For this reason, and also since an efficient code for the simulation of incompressible free flows and scalar elliptic problems is available [26], the use of iterative strategies is our preferred option.

Surveying the literature on iterative methods, one finds that depending on the splitting of the interface conditions, different strategies were proposed. This splitting defines the boundary condition on Γ_I for the individual Stokes and Darcy problems that have to be solved at each iteration. Principally, it is possible to perform the splitting such that essential, natural, or Robin (linear combination of essential and natural) boundary conditions on Γ_I can be prescribed. A first approach consists in using natural boundary conditions for the Stokes problems, i.e., (7), (9) or (7), (10), which involve Dirichlet data from the Darcy problem, and also natural conditions for the Darcy problems, i.e., (6), which use Dirichlet data from the Stokes problems, e.g., [27, 12]. Since this strategy results in Neumann problems to be solved in both subdomains, this approach will be called Neumann–Neumann coupled formulation. It is

worth noting that, from the point of view of domain decomposition methods, this strategy is often considered as of Dirichlet-to-Neumann type [27, 12]. However, the Neumann–Neumann coupling possesses some disadvantages. In particular, it has been shown that it converges very slowly on fine meshes for small values of the viscosity or the hydraulic conductivity [12], a configuration which is of utmost importance for applications in geosciences, where, e.g., $\nu = 10^{-6}$ $[m^2/s]$ (water) and $K \in [10^{-9}I, 10^{-3}I]$ $[m/s]$ (clay, sand, gravel), are values of interest.

To overcome these problems, it was first proposed in [12] to use a Robin–Robin coupling. The numerical results in [12] are very promising, showing that the Robin–Robin decomposition is robust and efficient in the parameter range that is of interest for geoscientific applications. The idea behind the Robin–Robin coupling for Stokes–Darcy problems is to solve Robin problems rather than Neumann problems in both subdomains, introducing two parameters γ_f and γ_p, which determine the linear combination of the essential and natural boundary condition for Stokes and Darcy problems, respectively. As shown in [12], these additional parameters have to be tuned in order to achieve fast convergence of the iterative scheme. Moreover, recent works showed that Robin boundary conditions can be seen, in the context of the finite element method, as a generalization of Neumann and Dirichlet conditions, without significant loss of accuracy and stability see, e.g., [28]. After the pioneering work of [12], more variants of Robin–Robin iterative methods have been proposed and analyzed, see, e.g., [4, 9, 16].

For motivating our work, the discussion of some details of the algorithms proposed in [12] and [16] is necessary. The sequential algorithm from [12] solves at each iteration a Darcy and a Stokes problem sequentially, i.e., updating after each step the boundary conditions on Γ_I using the latest solution available on the other subdomain. This approach corresponds to a Gauss–Seidel strategy for the solution of the coupled problem. The presented numerical analysis in [12] suggests that the Robin–Robin parameters should satisfy $\gamma_f > \gamma_p$ at least for ν, $K \ll 1$. The numerical studies considered the choice $\gamma_f = 0.3$ and $\gamma_p = 0.1$, showing robustness with respect to grid size, viscosity, and permeability, but restricted to the simplified interface condition (10) and $\nu < 10^{-4}$, $K < 10^{-3}$. In [9, 16], a very similar algorithm was analyzed, where the Stokes and the Darcy problem are solved simultaneously in each iteration, updating simultaneously also the boundary condition on Γ_I for both subproblems. This approach, called parallel algorithm in [16], is the canonical modification of the sequential (Gauss–Seidel) algorithm proposed in [12] to the Jacobi-type. In fact, one has to solve the same subproblems and the updates of the Robin boundary data at the interface have the same structure, see Section 3. The only difference between both algorithms is that in the definition of the Robin data for the Stokes problem, the solution of the Darcy problem is either from the current or from the previous iterate. In [16], the convergence was proved theoretically for $\gamma_f < \gamma_p$, for the Beaver–Joseph–Saffman condition (9), and any initial iterate. However, the numerical studies have been restricted to the value $\gamma_p = 1$, considering also unitary viscosity and permeability, $\nu = 1$, $K = 1$.

Hence, although the algorithms proposed in [12] and [16] differ only slightly, the analysis and the results presented in these papers suggest completely different choices of appropriate Robin–Robin parameters. This puzzling situation is of course unsatisfactory and it makes the usage of Robin–Robin coupling prohibitive in practical applications. In particular, several questions remain to be addressed, concerning the dependence of the numerical parameters on the coefficients of the problem.

One of the main contributions of this report consists in a unified presentation of the considered algorithms, thereby identifying the common underlying structure and highlighting their differences. In particular, it will be clarified that different updating strategies for the Robin conditions on the interface can be applied. One of them is based on rewriting the Neumann–Neumann formulation as a Robin–Robin formulation whereas the other one directly uses a Robin–Robin formulation of the coupled problem. The first approach leads, for standard finite element methods, to continuous data at the interface and the second one to discontinuous data. Another main contribution is the assessment of the algorithms for problems whose

coefficients are of the magnitude which is relevant for applications from geosciences. It will turn out that only one of the updating strategies will lead to efficient methods, if it is used with appropriately chosen parameters in the Robin boundary conditions. The size of appropriate parameters is considerably larger, at least in the studied examples, than proposed so far in the literature. The numerical studies also show that not only the size but also the ratio of appropriately chosen Robin parameters depends on the coefficients of the problem.

The remainder of the report is organized as follows. Section 2 introduces the variational and the finite element formulations of the coupled problems, while Section 3 focuses on the two iterative strategies considered in the report. Computational results are presented in Section 4, and Section 5 gives a summary and an outlook.

2. WEAK FORMULATION OF THE COUPLED STOKES–DARCY PROBLEM

The scope of this section is to introduce the basic notation and the weak formulations of the coupled Stokes–Darcy problem, considering different strategies to include the interface conditions.

2.1. Weak formulations

The first step of the numerical simulation of any physical model is its non-dimensionalization using characteristic scales. It will be assumed, without loss of generality, that the equations (1), (2), and (5) and the interface conditions (6), (7), and (9) (or (10)) are non-dimensionalized with unity characteristic scales such that the non-dimensional equations have exactly the same form. Moreover, as usual the Stokes pressure is defined such that it incorporates the density. For simplicity of presentation, our notation will not distinguish between dimensional and non-dimensional quantities.

Besides interface conditions on Γ_I, also boundary conditions on the external boundaries $(\partial \Omega_f \cup \partial \Omega_p) \setminus \Gamma_I$ have to be specified. In what follows, only homogeneous conditions will be considered. However, the presented arguments can be extended also to the general non-homogeneous case. For the Stokes problem, it is assumed that

$$\mathbf{u}_f = \mathbf{0} \text{ on } \Gamma_{f,e} \text{ (no-flow, essential boundary conditions)},$$

$$\mathbb{T}(\mathbf{u}_f, p_f) \cdot \mathbf{n} = \mathbf{0} \text{ on } \Gamma_{f,n} \text{ (outflow, natural boundary conditions)},$$

where $\Gamma_{f,e} \cup \Gamma_{f,n} = \partial \Omega_f \setminus \Gamma_I$ and $\Gamma_{f,e} \cap \Gamma_{f,n} = \emptyset$. For the Darcy problem, the boundary conditions are defined by

$$\varphi_p = 0 \text{ on } \Gamma_{p,e} \text{ (essential/Dirichlet)},$$

$$\mathbb{K} \nabla \varphi_p \cdot \mathbf{n} = 0 \text{ on } \Gamma_{p,n} \text{ (natural/Neumann)},$$

with $\Gamma_{p,e} \cup \Gamma_{p,n} = \partial \Omega_p \setminus \Gamma_I$ and $\Gamma_{p,e} \cap \Gamma_{p,n} = \emptyset$. Furthermore, the boundary parts where essential boundary conditions are prescribed are assumed to have positive measure, $|\Gamma_{f,e}| > 0$, $|\Gamma_{p,e}| > 0$.

For an open set $\omega \subset \mathbb{R}^d$, let $H^m(\omega)$ denote the standard Sobolev spaces and let $L^2(\omega) = H^0(\omega)$. In addition, $(\cdot, \cdot)_\omega$ denotes the $L^2(\omega)$ inner product and $\langle \cdot, \cdot \rangle_{\Gamma_I}$ stands for the inner product in $L^2(\Gamma_I)$.

For the derivation of a weak formulation, the essential boundary conditions are incorporated into the function spaces. Hence, the space for the Stokes velocity is given by

$$V_f = \left\{ \mathbf{v} \in \left(H^1(\Omega_f) \right)^d \ : \mathbf{v} = \mathbf{0} \text{ on } \Gamma_{f,e} \right\}.$$

The correct choice of the pressure space depends on the boundary conditions. If $\Gamma_{f,n} = \emptyset$, then the pressure is sought in the space

$$Q_f = L_0^2(\Omega_f) = \left\{ q \in L^2(\Omega_f) \ : \ \int_{\Omega_f} q \, d\mathbf{x} = 0 \right\},$$

otherwise in $Q_{\mathrm{f}} = L^2(\Omega_{\mathrm{f}})$. For the Darcy problem, the space for the piezometric head is defined by

$$Q_{\mathrm{p}} = \left\{ \psi \in H^1(\Omega_{\mathrm{p}}) \ : \ \psi = 0 \text{ on } \Gamma_{\mathrm{p},e} \right\}.$$

The weak formulations of the Stokes and the Darcy equations are derived in a standard way by multiplying (1), (2), and (5) with appropriate test functions and applying integration by parts. Due to the choice of the boundary conditions, all integrals on $(\partial\Omega_{\mathrm{f}} \cup \partial\Omega_{\mathrm{p}}) \setminus \Gamma_I$ vanish. One obtains the following weak form of the Stokes–Darcy problem: Find $(\mathbf{u}_{\mathrm{f}}, p_{\mathrm{f}}, \varphi_{\mathrm{p}}) \in V_{\mathrm{f}} \times Q_{\mathrm{f}} \times Q_{\mathrm{p}}$ such that for all $(\mathbf{v}, q, \psi) \in V_{\mathrm{f}} \times Q_{\mathrm{f}} \times Q_{\mathrm{p}}$

$$(\mathbb{T}(\mathbf{u}_{\mathrm{f}}, p_{\mathrm{f}}), \mathbb{D}(\mathbf{v}))_{\Omega_{\mathrm{f}}} + (\nabla \cdot \mathbf{u}_{\mathrm{f}}, q)_{\Omega_{\mathrm{f}}} - \langle \mathbb{T}(\mathbf{u}_{\mathrm{f}}, p_{\mathrm{f}}) \cdot \mathbf{n}_{\mathrm{f}}, \mathbf{v} \rangle_{\Gamma_I} \ = \ (\mathbf{f}_{\mathrm{f}}, \mathbf{v})_{\Omega_{\mathrm{f}}}, \tag{11}$$

$$(\mathbb{K}\nabla\varphi_{\mathrm{p}}, \nabla\psi)_{\Omega_{\mathrm{p}}} + \langle \mathbb{K}\nabla\varphi_{\mathrm{p}} \cdot \mathbf{n}_{\mathrm{f}}, \psi \rangle_{\Gamma_I} \ = \ (f_{\mathrm{p}}, \psi)_{\Omega_{\mathrm{p}}}. \tag{12}$$

The Beavers–Joseph–Saffman condition (9) can be naturally included into the weak formulation (11) decomposing the integral over Γ_I in (11) into normal and tangential components, yielding

$$-\langle \mathbb{T}(\mathbf{u}_{\mathrm{f}}, p_{\mathrm{f}}) \cdot \mathbf{n}_{\mathrm{f}}, \mathbf{v} \rangle_{\Gamma_I} = -\langle \mathbf{n}_{\mathrm{f}} \cdot \mathbb{T}(\mathbf{u}_{\mathrm{f}}, p_{\mathrm{f}}) \cdot \mathbf{n}_{\mathrm{f}}, \mathbf{v} \cdot \mathbf{n}_{\mathrm{f}} \rangle_{\Gamma_I} - \sum_{i=1}^{d-1} \underbrace{\langle \boldsymbol{\tau}_i \cdot \mathbb{T}(\mathbf{u}_{\mathrm{f}}, p_{\mathrm{f}}) \cdot \mathbf{n}_{\mathrm{f}}, \mathbf{v} \cdot \boldsymbol{\tau}_i \rangle_{\Gamma_I}}_{=-\frac{1}{\alpha}\langle \mathbf{u}_{\mathrm{f}} \cdot \boldsymbol{\tau}_i, \mathbf{v} \cdot \boldsymbol{\tau}_i \rangle_{\Gamma_I}}.$$

Rearranging terms leads to

$$a_{\mathrm{f}}(\mathbf{u}_{\mathrm{f}}, \mathbf{v}) + b_{\mathrm{f}}(\mathbf{v}, p_{\mathrm{f}}) - b_{\mathrm{f}}(\mathbf{u}_{\mathrm{f}}, q) - \langle \mathbf{n}_{\mathrm{f}} \cdot \mathbb{T}(\mathbf{u}_{\mathrm{f}}, p_{\mathrm{f}}) \cdot \mathbf{n}_{\mathrm{f}}, \mathbf{v} \cdot \mathbf{n}_{\mathrm{f}} \rangle_{\Gamma_I} = (\mathbf{f}_{\mathrm{f}}, \mathbf{v})_{\Omega_{\mathrm{f}}}, \tag{13}$$

$$a_{\mathrm{p}}(\varphi_{\mathrm{p}}, \psi) + \langle \mathbb{K}\nabla\varphi_{\mathrm{p}} \cdot \mathbf{n}_{\mathrm{f}}, \psi \rangle_{\Gamma_I} = (f_{\mathrm{p}}, \psi)_{\Omega_{\mathrm{p}}}, \tag{14}$$

with $a_{\mathrm{f}} : V_{\mathrm{f}} \times V_{\mathrm{f}} \to \mathbb{R}$, $b_{\mathrm{f}} : V_{\mathrm{f}} \times Q_{\mathrm{f}} \to \mathbb{R}$, and $a_{\mathrm{p}} : Q_{\mathrm{p}} \times Q_{\mathrm{p}} \to \mathbb{R}$ defined by

$$a_{\mathrm{f}}(\mathbf{u}, \mathbf{v}) = (2\nu\mathbb{D}(\mathbf{u}), \mathbb{D}(\mathbf{v}))_{\Omega_{\mathrm{f}}} + \sum_{i=1}^{d-1} \frac{1}{\alpha} \langle \mathbf{u} \cdot \boldsymbol{\tau}_i, \mathbf{v} \cdot \boldsymbol{\tau}_i \rangle_{\Gamma_I},$$

$$b_{\mathrm{f}}(\mathbf{v}, p) = -(\nabla \cdot \mathbf{v}, p)_{\Omega_{\mathrm{f}}},$$

$$a_{\mathrm{p}}(\varphi, \psi) = (\mathbb{K}\nabla\varphi, \nabla\psi)_{\Omega_{\mathrm{p}}}.$$

In the case of the simplified interface condition (10), one obtains equations of the same form as (13)–(14) with the following bilinear form

$$a_{\mathrm{f}}(\mathbf{u}, \mathbf{v}) = (2\nu\mathbb{D}(\mathbf{u}), \mathbb{D}(\mathbf{v}))_{\Omega_{\mathrm{f}}} - \sum_{i=1}^{d-1} \langle \boldsymbol{\tau}_i \cdot \mathbb{T}(\mathbf{u}_{\mathrm{f}}, p_{\mathrm{f}}) \cdot \mathbf{n}_{\mathrm{f}}, \mathbf{v} \cdot \boldsymbol{\tau}_i \rangle_{\Gamma_I},$$

where the second term does not vanish in the case of weakly imposed boundary conditions, see Section 3.3.

2.2. Neumann–Neumann coupled formulation

For completeness of presentation and for highlighting the differences to the Robin–Robin formulation, first the Neumann–Neumann coupled formulation is reviewed. Inserting the interface conditions (7) and (6) into (13)–(14) yields the coupled Stokes–Darcy weak formulation

$$a_{\mathrm{f}}(\mathbf{u}_{\mathrm{f}}, \mathbf{v}) + b_{\mathrm{f}}(\mathbf{v}, p_{\mathrm{f}}) - b_{\mathrm{f}}(\mathbf{u}_{\mathrm{f}}, q) + \langle g\varphi_{\mathrm{p}}, \mathbf{v} \cdot \mathbf{n}_{\mathrm{f}} \rangle_{\Gamma_I} = (\mathbf{f}_{\mathrm{f}}, \mathbf{v})_{\Omega_{\mathrm{f}}}, \tag{15}$$

$$a_{\mathrm{p}}(\varphi_{\mathrm{p}}, \psi) - \langle \mathbf{u}_{\mathrm{f}} \cdot \mathbf{n}_{\mathrm{f}}, \psi \rangle_{\Gamma_I} = (f_{\mathrm{p}}, \psi)_{\Omega_{\mathrm{p}}}. \tag{16}$$

Here, the coupling is based on Neumann interface conditions for both the Stokes and the Darcy domain, and (15)–(16) will be therefore called a Neumann–Neumann coupled problem.

In order to describe better the different coupled formulations arising from the Stokes–Darcy problem, it is helpful to rewrite (15)–(16) in a more abstract form. Let $\mathcal{V}_\mathrm{f} = (V_\mathrm{f}, Q_\mathrm{f})$ be the function space in which the solution (velocity and pressure) to the Stokes problem is sought, and let $\mathcal{V}_\mathrm{f}'$ denote its dual space. Similarly, let Q_p' denote the dual of Q_p. Then, define the operators $\mathcal{S} : \mathcal{V}_\mathrm{f} \to \mathcal{V}_\mathrm{f}'$ and $\mathcal{D} : Q_\mathrm{p} \to Q_\mathrm{p}'$ such that

$$(\mathcal{D}\varphi, \psi) := a_\mathrm{p}(\varphi, \psi),$$
$$(\mathcal{S}s, t) := a_\mathrm{f}(\mathbf{u}, \mathbf{v}) + b_\mathrm{f}(\mathbf{v}, p) - b_\mathrm{f}(\mathbf{u}, q),$$

for all $s = (\mathbf{u}, p)$, $t = (\mathbf{v}, q) \in \mathcal{V}_\mathrm{f}$, and $\varphi, \psi \in Q_\mathrm{p}$, and the coupling operator $\mathcal{C} : \mathcal{V}_\mathrm{f} \to Q_\mathrm{p}'$ by

$$(\mathcal{C}s, \psi) := \langle \mathbf{u} \cdot \mathbf{n}_\mathrm{f}, \psi \rangle_{\Gamma_\mathrm{I}}.$$

Then, the Neumann–Neumann coupled problem (15)–(16) can be equivalently written as: Find $\varphi \in Q_\mathrm{p}$ and $s = (\mathbf{u}, p) \in \mathcal{V}_\mathrm{f}$ such that

$$\begin{pmatrix} \mathcal{D} & -\mathcal{C} \\ g\mathcal{C}^\top & \mathcal{S} \end{pmatrix} \begin{pmatrix} \varphi \\ s \end{pmatrix} = \begin{pmatrix} \mathcal{F}_\mathrm{p} \\ \mathcal{F}_\mathrm{f} \end{pmatrix}. \tag{17}$$

The operator $\mathcal{C}^\top : Q_\mathrm{p} \to \mathcal{C}_\mathrm{f}'$ is the adjoint of $\mathcal{C}$ and the right-hand sides $\mathcal{F}_\mathrm{f} \in \mathcal{V}_\mathrm{f}'$ and $\mathcal{F}_\mathrm{p} \in Q_\mathrm{p}'$ are defined by

$$(\mathcal{F}_\mathrm{p}, \psi) := (f_\mathrm{p}, \psi)_{\Omega_\mathrm{p}}, \qquad (\mathcal{F}_\mathrm{f}, t) := (\mathbf{f}_\mathrm{f}, \mathbf{v})_{\Omega_\mathrm{f}},$$

for all $t = (\mathbf{v}, q) \in \mathcal{V}_\mathrm{f}$ and all $\psi \in Q_\mathrm{p}$. An equivalent form of the coupled Stokes–Darcy system can be obtained using Lagrange multipliers on the interface Γ_I. This approach allows to formally decouple the Stokes and the Darcy subproblems, introducing additional interface variables $\eta_\mathrm{f}, \eta_\mathrm{p} \in H^{1/2}(\Gamma_\mathrm{I})$, and considering the system

$$\begin{pmatrix} \mathcal{D} & & & -\mathcal{E}_\mathrm{p} \\ \mathcal{R}_\mathrm{p} & -\mathcal{I} & & \\ & -\mathcal{E}_\mathrm{f} & \mathcal{S} & \\ & & \mathcal{R}_\mathrm{f} & -\mathcal{I} \end{pmatrix} \begin{pmatrix} \varphi \\ \eta_f \\ s \\ \eta_p \end{pmatrix} = \begin{pmatrix} \mathcal{F}_\mathrm{p} \\ 0 \\ \mathcal{F}_\mathrm{f} \\ 0 \end{pmatrix} \in \begin{pmatrix} Q_\mathrm{p}' \\ H^{1/2}(\Gamma_\mathrm{I}) \\ \mathcal{V}_\mathrm{f}' \\ H^{1/2}(\Gamma_\mathrm{I}) \end{pmatrix}, \tag{18}$$

where $\mathcal{I}$ is the identity operator on $H^{1/2}(\Gamma_\mathrm{I})$,

$$\mathcal{E}_\mathrm{f} : H^{1/2}(\Gamma_\mathrm{I}) \to \mathcal{V}_\mathrm{f}', \qquad\qquad (\mathcal{E}_\mathrm{f}\eta_\mathrm{f}, t) = \langle \eta_\mathrm{f}, \mathbf{v} \cdot \mathbf{n}_\mathrm{f} \rangle_{\Gamma_\mathrm{I}},$$
$$\mathcal{E}_\mathrm{p} : H^{1/2}(\Gamma_\mathrm{I}) \to Q_\mathrm{p}', \qquad\qquad (\mathcal{E}_\mathrm{p}\eta_\mathrm{p}, \psi) = \langle \eta_\mathrm{p}, \psi \rangle_{\Gamma_\mathrm{I}},$$

correspond to extension operators into the Stokes and Darcy domain, respectively, and

$$\mathcal{R}_\mathrm{p} : Q_\mathrm{p} \to H^{1/2}(\Gamma_\mathrm{I}), \qquad\qquad \psi \mapsto g\psi\big|_{\Gamma_\mathrm{I}},$$
$$\mathcal{R}_\mathrm{f} : \mathcal{V}_\mathrm{f} \to H^{1/2}(\Gamma_\mathrm{I}), \qquad\qquad t \mapsto \mathbf{v}\big|_{\Gamma_\mathrm{I}} \cdot \mathbf{n}_\mathrm{f},$$

are restriction operators on $H^{1/2}(\Gamma_\mathrm{I})$ from the two subdomains. The formulation (18) is equivalent to (17) since, by definition,

$$g\mathcal{C}^\top = -\mathcal{E}_\mathrm{f}\mathcal{R}_\mathrm{p} \quad \text{and} \quad \mathcal{C} = \mathcal{E}_\mathrm{p}\mathcal{R}_\mathrm{f}.$$

2.3. Robin–Robin coupled formulation

Instead of the interface conditions (6) and (7) one can as well consider two linear combinations

$$\gamma_\mathrm{f}\mathbf{u}_\mathrm{f} \cdot \mathbf{n}_\mathrm{f} + \mathbf{n}_\mathrm{f} \cdot \mathbb{T}(\mathbf{u}_\mathrm{f}, p_\mathrm{f}) \cdot \mathbf{n}_\mathrm{f} = -\gamma_\mathrm{f}\mathbb{K}\nabla\varphi_\mathrm{p} \cdot \mathbf{n}_\mathrm{f} - g\varphi_\mathrm{p} \qquad\qquad \text{on } \Gamma_\mathrm{I}, \tag{19}$$
$$\gamma_\mathrm{p}\mathbb{K}\nabla\varphi_\mathrm{p} \cdot \mathbf{n}_\mathrm{f} - g\varphi_\mathrm{p} = -\gamma_\mathrm{p}\mathbf{u}_\mathrm{f} \cdot \mathbf{n}_\mathrm{f} + \mathbf{n}_\mathrm{f} \cdot \mathbb{T}(\mathbf{u}_\mathrm{f}, p_\mathrm{f}) \cdot \mathbf{n}_\mathrm{f} \qquad \text{on } \Gamma_\mathrm{I}, \tag{20}$$

where $\gamma_\mathrm{f} \geq 0$ and $\gamma_\mathrm{p} > 0$ are constant. The conditions (19) and (20) correspond to Robin boundary conditions for the Stokes and Darcy subproblems, respectively. Inserting them into the weak formulations (13)–(14) leads to

$$a_\mathrm{f}(\mathbf{u}_\mathrm{f}, \mathbf{v}) + b_\mathrm{f}(\mathbf{v}, p_\mathrm{f}) - b_\mathrm{f}(\mathbf{u}_\mathrm{f}, q)$$
$$+ \langle \gamma_\mathrm{f}\mathbf{u}_\mathrm{f} \cdot \mathbf{n}_\mathrm{f}, \mathbf{v} \cdot \mathbf{n}_\mathrm{f} \rangle_{\Gamma_\mathrm{I}} + \langle g\varphi_\mathrm{p}, \mathbf{v} \cdot \mathbf{n} \rangle_{\Gamma_\mathrm{I}} + \langle \gamma_\mathrm{f}\mathbb{K}\nabla\varphi_\mathrm{p} \cdot \mathbf{n}_\mathrm{f}, \mathbf{v} \cdot \mathbf{n}_\mathrm{f} \rangle_{\Gamma_\mathrm{I}} = (\mathbf{f}_\mathrm{f}, \mathbf{v})_{\Omega_\mathrm{f}}, \quad (21)$$

$$a_\mathrm{p}(\varphi_\mathrm{p}, \psi) + \left\langle \frac{1}{\gamma_\mathrm{p}}g\varphi_\mathrm{p}, \psi \right\rangle_{\Gamma_\mathrm{I}} + \left\langle \frac{1}{\gamma_\mathrm{p}}\mathbf{n}_\mathrm{f} \cdot \mathbb{T}(\mathbf{u}_\mathrm{f}, p_\mathrm{f}) \cdot \mathbf{n}_\mathrm{f}, \psi \right\rangle_{\Gamma_\mathrm{I}} - \langle \mathbf{u}_\mathrm{f} \cdot \mathbf{n}_\mathrm{f}, \psi \rangle_{\Gamma_\mathrm{I}} = (f_\mathrm{p}, \psi)_{\Omega_\mathrm{p}}, \quad (22)$$

which will be denoted as the Robin–Robin coupled formulation. The restrictions $\gamma_\mathrm{f} \geq 0$ and $\gamma_\mathrm{p} > 0$ guarantee positiveness of the bilinear forms $a_\mathrm{f}(\mathbf{u}_\mathrm{f}, \mathbf{v}) + \langle \gamma_\mathrm{f}\mathbf{u}_\mathrm{f} \cdot \mathbf{n}_\mathrm{f}, \mathbf{v} \cdot \mathbf{n}_\mathrm{f} \rangle_{\Gamma_\mathrm{I}}$ and $a_\mathrm{p}(\varphi_\mathrm{p}, \psi) + \left\langle \frac{1}{\gamma_\mathrm{p}}g\varphi_\mathrm{p}, \psi \right\rangle_{\Gamma_\mathrm{I}}$. Introducing the operators $\mathcal{S}_{\Gamma_\mathrm{I}} : \mathcal{V}_\mathrm{f} \to \mathcal{V}_\mathrm{f}'$, $\mathcal{D}_{\Gamma_\mathrm{I}} : Q_\mathrm{p} \to Q_\mathrm{p}'$, $\mathcal{C}_\mathrm{p} : \mathcal{V}_\mathrm{f} \to Q_\mathrm{p}'$, and $\mathcal{C}_\mathrm{f}^\top : Q_\mathrm{p} \to \mathcal{V}_\mathrm{f}'$ defined by

$$(\mathcal{S}_{\Gamma_\mathrm{I}}s, t) = \langle \mathbf{u} \cdot \mathbf{n}_\mathrm{f}, \mathbf{v} \cdot \mathbf{n}_\mathrm{f} \rangle_{\Gamma_\mathrm{I}},$$
$$(\mathcal{D}_{\Gamma_\mathrm{I}}\varphi, \psi) = \langle g\varphi_\mathrm{p}, \psi \rangle_{\Gamma_\mathrm{I}},$$
$$(\mathcal{C}_\mathrm{f}^\top \varphi, t) = \langle \mathbb{K}\nabla\varphi \cdot \mathbf{n}_\mathrm{f}, \mathbf{v} \cdot \mathbf{n}_\mathrm{f} \rangle_{\Gamma_\mathrm{I}},$$
$$(\mathcal{C}_\mathrm{p}s, \psi) = \langle \mathbf{n}_\mathrm{f} \cdot \mathbb{T}(\mathbf{u}, p) \cdot \mathbf{n}_\mathrm{f}, \psi \rangle_{\Gamma_\mathrm{I}},$$

for all $s = (\mathbf{u}, p) \in \mathcal{V}_\mathrm{f}$, $t = (\mathbf{v}, q) \in \mathcal{V}_\mathrm{f}$, $\varphi, \psi \in Q_\mathrm{p}$, one can rewrite (21)–(22) as

$$\begin{pmatrix} \mathcal{D}_\mathrm{rob} & \mathcal{C}_\mathrm{rob} \\ \mathcal{C}_\mathrm{rob}^\top & \mathcal{S}_\mathrm{rob} \end{pmatrix} \begin{pmatrix} \varphi \\ s \end{pmatrix} := \left(\begin{pmatrix} \mathcal{D} & -\mathcal{C} \\ g\mathcal{C}^\top & \mathcal{S} \end{pmatrix} + \begin{pmatrix} \gamma_\mathrm{p}^{-1} & \\ & \gamma_\mathrm{f} \end{pmatrix} \begin{pmatrix} \mathcal{D}_{\Gamma_\mathrm{I}} & \mathcal{C}_\mathrm{p} \\ \mathcal{C}_\mathrm{f}^\top & \mathcal{S}_{\Gamma_\mathrm{I}} \end{pmatrix} \right) \begin{pmatrix} \varphi \\ s \end{pmatrix} = \begin{pmatrix} \mathcal{F}_\mathrm{p} \\ \mathcal{F}_\mathrm{f} \end{pmatrix}. \quad (23)$$

The second term represents the additional operators in the Robin–Robin problem (21)–(22) in comparison with the Neumann–Neumann formulation (15)–(16), compare also with (17).

Remark 2.1
The resulting coupled weak formulations (15)–(16) and (21)–(22) are equivalent if and only if $V_\mathrm{f} \cdot \mathbf{n}_\mathrm{f}\big|_{\Gamma_\mathrm{I}} = Q_\mathrm{p}\big|_{\Gamma_\mathrm{I}}$. This equality is satisfied if $\Gamma_{\mathrm{f},e} \cap \Gamma_\mathrm{I} = \Gamma_{\mathrm{p},e} \cap \Gamma_\mathrm{I}$, i.e., if the types of boundary conditions (essential/natural), imposed on the intersection between interface and outer boundary, coincide.

Similarly to the Neumann–Neumann case one introduces two interface variables $\eta_\mathrm{f}, \eta_\mathrm{p} \in H^{-1/2}(\Gamma_\mathrm{I})$ and considers the system

$$\begin{pmatrix} \mathcal{D}_\mathrm{rob} & & & -\mathcal{E}_\mathrm{p} \\ \mathcal{R}_\mathrm{p,rob} & -\mathcal{I} & & \\ & -\mathcal{E}_\mathrm{f} & \mathcal{S}_\mathrm{rob} & \\ & & \mathcal{R}_\mathrm{f,rob} & -\mathcal{I} \end{pmatrix} \begin{pmatrix} \varphi \\ \eta_f \\ s \\ \eta_p \end{pmatrix} = \begin{pmatrix} \mathcal{F}_\mathrm{p} \\ 0 \\ \mathcal{F}_\mathrm{f} \\ 0 \end{pmatrix} \in \begin{pmatrix} Q_\mathrm{p}' \\ H^{-1/2}(\Gamma_\mathrm{I}) \\ \mathcal{V}_\mathrm{f}' \\ H^{-1/2}(\Gamma_\mathrm{I}) \end{pmatrix}, \quad (24)$$

where $\mathcal{I}$ is the identity operator on $H^{-1/2}(\Gamma_\mathrm{I})$. Then, one defines for all $t = (\mathbf{v}, q) \in \mathcal{V}_\mathrm{f}$ and all $\psi \in Q_\mathrm{p}$:

$$\mathcal{R}_\mathrm{p,rob} : Q_\mathrm{p} \to H^{-1/2}(\Gamma_\mathrm{I}), \qquad \psi \mapsto (g\psi + \gamma_\mathrm{f}\mathbb{K}\nabla\psi \cdot \mathbf{n}_\mathrm{f})\big|_{\Gamma_\mathrm{I}},$$
$$\mathcal{R}_\mathrm{f,rob} : \mathcal{V}_\mathrm{f} \to H^{-1/2}(\Gamma_\mathrm{I}), \qquad t \mapsto (\gamma_\mathrm{p}^{-1}\mathbf{n}_\mathrm{f} \cdot \mathbb{T}(\mathbf{v}, q) - \mathbf{v})\big|_{\Gamma_\mathrm{I}} \cdot \mathbf{n}_\mathrm{f}.$$

In (24), the operators $\mathcal{E}_\mathrm{p}$ and $\mathcal{E}_\mathrm{f}$ are defined on $H^{-1/2}(\Gamma_\mathrm{I})$. By construction, (24) is equivalent to (23), since

$$\mathcal{C}_\mathrm{rob}^\top = -\mathcal{E}_\mathrm{f}\mathcal{R}_\mathrm{p,rob} \quad \text{and} \quad \mathcal{C}_\mathrm{rob} = \mathcal{E}_\mathrm{p}\mathcal{R}_\mathrm{f,rob}.$$

2.4. A Robin–Robin formulation for the Neumann–Neumann problem

In the context of finite element methods, computing derivatives of discrete functions in general leads to loss of approximation orders. Hence, the Robin–Robin formulation might result in a suboptimal accuracy. On the other hand, Robin boundary conditions allow for additional flexibility at the interface and they can give efficient algorithms as reported in [12]. An alternative weak formulation, equivalent to the Neumann–Neumann formulation (17), but based on the solution of two Robin problems in the subdomains Ω_f and Ω_p, which do not require the computation of derivatives, has been proposed in [12, 16] in the context of subdomain iterative methods. Using the framework introduced above, this coupled formulation can be written in the form

$$
\begin{pmatrix}
\mathcal{D} + \gamma_\mathrm{p}^{-1}\mathcal{D}_{\Gamma_\mathrm{I}} & & & -\gamma_\mathrm{p}^{-1}\mathcal{E}_\mathrm{p} \\
b\mathcal{R}_\mathrm{p} & -\mathcal{I} & & a\mathcal{I} \\
& -\mathcal{E}_\mathrm{f} & \mathcal{S} + \gamma_\mathrm{f}\mathcal{S}_{\Gamma_\mathrm{I}} & \\
& c\mathcal{I} & d\mathcal{R}_\mathrm{f} & -\mathcal{I}
\end{pmatrix}
\begin{pmatrix}
\varphi \\ \eta_f \\ s \\ \eta_p
\end{pmatrix}
=
\begin{pmatrix}
\mathcal{F}_\mathrm{p} \\ 0 \\ \mathcal{F}_\mathrm{f} \\ 0
\end{pmatrix},
\tag{25}
$$

where the factors a, b, c, and d have to be determined in order to obtain a formulation equivalent to (17) (and to (18)). The choice of the form (25) is motivated by two reasons. Firstly, it prevents the subproblems to be coupled directly (first and third row). An indirect coupling is enforced only through the interface functions η_f and η_p (for the Stokes and Darcy problem, respectively). Secondly, each interface function can be computed from the solution in a single subdomain (empty blocks in the second and fourth row). The signs of the operators and the positions of γ_f and γ_p are chosen such that the resulting scheme will coincide with the ones presented in [12, 16]. System (25) is equivalent to (17) if

$$
\begin{pmatrix}
\mathcal{D} + \gamma_\mathrm{p}^{-1}\mathcal{D}_{\Gamma_\mathrm{I}} & & & -\gamma_\mathrm{p}^{-1}\mathcal{E}_\mathrm{p} \\
b\mathcal{R}_\mathrm{p} & -\mathcal{I} & & a\mathcal{I} \\
& -\mathcal{E}_\mathrm{f} & \mathcal{S} + \gamma_\mathrm{f}\mathcal{S}_{\Gamma_\mathrm{I}} & \\
& c\mathcal{I} & d\mathcal{R}_\mathrm{f} & -\mathcal{I}
\end{pmatrix}
\begin{pmatrix}
\varphi \\ \eta_f \\ s \\ \eta_p
\end{pmatrix}
=
\begin{pmatrix}
\mathcal{D} & & -\mathcal{C} \\
& & \\
\mathcal{C}^\top & & \mathcal{S}
\end{pmatrix}
\begin{pmatrix}
\varphi \\ 0 \\ s \\ 0
\end{pmatrix}
=
\begin{pmatrix}
\mathcal{F}_\mathrm{p} \\ 0 \\ \mathcal{F}_\mathrm{f} \\ 0
\end{pmatrix}
$$

$$
\iff
\begin{pmatrix}
\gamma_\mathrm{p}^{-1}\mathcal{D}_{\Gamma_\mathrm{I}} & & \mathcal{C} & -\gamma_\mathrm{p}^{-1}\mathcal{E}_\mathrm{p} \\
b\mathcal{R}_\mathrm{p} & -\mathcal{I} & & a\mathcal{I} \\
-\mathcal{C}^\top & -\mathcal{E}_\mathrm{f} & \gamma_\mathrm{f}\mathcal{S}_{\Gamma_\mathrm{I}} & \\
& c\mathcal{I} & d\mathcal{R}_\mathrm{f} & -\mathcal{I}
\end{pmatrix}
\begin{pmatrix}
\varphi \\ \eta_f \\ s \\ \eta_p
\end{pmatrix}
= 0,
$$

which yields the conditions

$$
\begin{cases}
\eta_\mathrm{p} = \gamma_\mathrm{p}\mathbf{u} \cdot \mathbf{n}_\mathrm{f} + g\varphi & \text{in } \Lambda_\mathrm{p}', \\
\eta_\mathrm{f} = bg\varphi + a\eta_\mathrm{p} & \text{in } H^{1/2}(\Gamma_\mathrm{I}), \\
\eta_\mathrm{f} = \gamma_\mathrm{f}\mathbf{u} \cdot \mathbf{n}_\mathrm{f} - g\varphi & \text{in } \Lambda_\mathrm{f}', \\
\eta_\mathrm{p} = d\mathbf{u} \cdot \mathbf{n}_\mathrm{f} + c\eta_\mathrm{f} & \text{in } H^{1/2}(\Gamma_\mathrm{I}),
\end{cases}
\tag{26}
$$

with the interface (trace) spaces

$$
\Lambda_\mathrm{f} := \mathbf{V}_\mathrm{f} \cdot \mathbf{n}_\mathrm{f}\big|_{\Gamma_\mathrm{I}} = \{\mathbf{v}|_{\Gamma_\mathrm{I}} \cdot \mathbf{n}_\mathrm{f} \ : \ \mathbf{v} \in \mathbf{V}_\mathrm{f}\} \text{ and } \Lambda_\mathrm{p} := Q_\mathrm{p}\big|_{\Gamma_\mathrm{I}} = \{\psi|_{\Gamma_\mathrm{I}} \ : \ \psi \in Q_\mathrm{p}\}.
$$

Remark 2.2
If the interface spaces Λ_f and Λ_p coincide, one can solve (26) for a, b, c, d, obtaining

$$
a = \frac{\gamma_\mathrm{f}}{\gamma_\mathrm{p}}, \qquad b = -1 - a, \qquad c = -1, \qquad d = \gamma_\mathrm{f} + \gamma_\mathrm{p},
$$

as done in [16]. This is the same condition as in Remark 2.1. If the interface spaces are not equal, we still use these parameters in the numerical simulations.

Remark 2.3
The difference between the two Robin–Robin formulations is that (23) is derived starting from two Robin subproblems in strong form, i.e., (19) and (20), while (25) is equivalent to two Robin problems obtained from the Neumann–Neumann strong form (15)–(16).

Remark 2.4
Unlike the Neumann–Neumann approach (18) and the Robin–Robin approach (24), the Robin–Robin formulation (26) can only be written in operator form using Lagrange multipliers, as the interface variables η_f and η_p are coupled to each other.

3. ROBIN–ROBIN SUBDOMAIN ITERATIVE METHODS

In the literature, one can find so-called sequential and parallel Robin–Robin subdomain iterative methods. This section starts by presenting the principal form of these algorithms. Then, the important issue of the definition of the boundary data at the interface will be considered. Finally, some details concerning the implementation of the algorithms will be presented and possible stopping criteria of the iterative process will be discussed.

3.1. Sequential and parallel approaches

The considered sequential form of the iterative method was proposed and studied, e.g., in [10, 12].

Algorithm S. (Sequential or Gauss–Seidel-type iteration)

0. Given $\eta_\mathrm{p}^0, \eta_\mathrm{f}^0 \in L^2(\Gamma_\mathrm{I})$, $\gamma_\mathrm{f} \geq 0$, $\gamma_\mathrm{p} > 0$, $\theta \in (0,1]$. Set $k = 0$.
1. Solve a Darcy problem with Robin boundary data η_p^k giving the solution φ_p^{k+1}.
2. Set η_f^{k+1} as a linear combination of η_f^k, η_p^k, and the solution of the Darcy problem by using the damping factor θ.
3. Solve a Stokes problem with Robin boundary data η_f^{k+1} giving the solution $(\mathbf{u}_\mathrm{f}^{k+1}, p_\mathrm{f}^{k+1})$.
4. Set η_p^{k+1} as a linear combination of η_p^k, η_f^{k+1}, and the solution of the Stokes problem by using the damping factor θ.
5. If not converged: Increase k by 1 and go to step 1.

A straightforward modification of Algorithm S into a version where the subproblems are solved in parallel was studied in [16].

Algorithm P. (Parallel or Jacobi-type iteration)

0. Given $\eta_\mathrm{f}^0, \eta_\mathrm{p}^0 \in L^2(\Gamma_\mathrm{I})$, $\gamma_\mathrm{f} \geq 0$, $\gamma_\mathrm{p} > 0$, $\theta \in (0,1]$. Set $k = 0$.
1. Do in parallel:
    a) Solve a Darcy problem with Robin boundary data η_p^k giving the solution φ_p^{k+1}.
    b) Solve a Stokes problem with Robin boundary data η_f^k giving the solution $(\mathbf{u}_\mathrm{f}^{k+1}, p_\mathrm{f}^{k+1})$.
2. Do in parallel:
    a) Set η_f^{k+1} as a linear combination of η_p^k, η_f^k, and the solution of the Darcy problem by using the damping factor θ.
    b) Set η_p^{k+1} as a linear combination of η_p^k, η_f^k, and the solution of the Stokes problem by using the damping factor θ.
3. If not converged: Increase k by 1 and go to step 1.

Note that in [10, 12, 16] the undamped versions, i.e., $\theta = 1$, were considered.
The Robin problems to be solved in Algorithms S and P have the form

- Darcy: Find $\varphi_{\mathrm{p}}^{k+1} \in Q_{\mathrm{p}}$ such that for all $\psi \in Q_{\mathrm{p}}$

$$a_{\mathrm{p}}\big(\varphi_{\mathrm{p}}^{k+1}, \psi\big) + \left\langle \frac{1}{\gamma_{\mathrm{p}}} g \varphi_{\mathrm{p}}^{k+1}, \psi \right\rangle_{\Gamma_{\mathrm{I}}} = (f_{\mathrm{p}}, \psi)_{\Omega_{\mathrm{p}}} + \left\langle \frac{1}{\gamma_{\mathrm{p}}} \eta_{\mathrm{p}}^{k}, \psi \right\rangle_{\Gamma_{\mathrm{I}}},$$

- Stokes: Find $(\mathbf{u}_{\mathrm{f}}^{k+1}, p_{\mathrm{f}}^{k+1}) \in V_{\mathrm{f}} \times Q_{\mathrm{f}}$ such that for all $(\mathbf{v}, q) \in V_{\mathrm{f}} \times Q_{\mathrm{f}}$

$$a_{\mathrm{f}}\big(\mathbf{u}_{\mathrm{f}}^{k+1}, \mathbf{v}\big) + b_{\mathrm{f}}\big(\mathbf{v}, p_{\mathrm{f}}^{k+1}\big) - b_{\mathrm{f}}\big(\mathbf{u}_{\mathrm{f}}^{k+1}, q\big) + \left\langle \gamma_{\mathrm{f}} \mathbf{u}_{\mathrm{f}}^{k+1} \cdot \mathbf{n}_{\mathrm{f}}, \mathbf{v} \cdot \mathbf{n}_{\mathrm{f}} \right\rangle_{\Gamma_{\mathrm{I}}}$$
$$= (\mathbf{f}_{\mathrm{f}}, \mathbf{v})_{\Omega_{\mathrm{f}}} + \left\langle \eta_{\mathrm{f}}^{\tilde{k}}, \mathbf{v} \cdot \mathbf{n}_{\mathrm{f}} \right\rangle_{\Gamma_{\mathrm{I}}},$$

where in Algorithm S it is $\tilde{k} = k+1$ and in Algorithm P it is $\tilde{k} = k$.

The matrix-vector representation of the two Robin–Robin formulations (24) and (25) possesses the structure

$$\begin{pmatrix} A_{11} & A_{12} \\ A_{21} & A_{22} \end{pmatrix} \begin{pmatrix} \begin{pmatrix} \varphi \\ \eta_{\mathrm{f}} \end{pmatrix} \\ \begin{pmatrix} s \\ \eta_{\mathrm{p}} \end{pmatrix} \end{pmatrix} = \begin{pmatrix} \begin{pmatrix} \mathcal{F}_{\mathrm{p}} \\ 0 \end{pmatrix} \\ \begin{pmatrix} \mathcal{F}_{\mathrm{f}} \\ 0 \end{pmatrix} \end{pmatrix}.$$

It can be seen that Algorithm S is a block Gauss–Seidel method (with a forward solve) for this system, whereas Algorithm P is a block Jacobi method, both methods are not damped. Moreover, both algorithms solve the subproblems involving the diagonal blocks A_{ii}, $i \in \{1, 2\}$, with one Gauss–Seidel step. Note that the subblocks A_{ii}, $i \in \{1, 2\}$, are lower triangular two-by-two block matrices themselves, with one diagonal block typically much bigger than the other one. Hence, Algorithm P is strictly speaking a nested Jacobi and Gauss–Seidel algorithm.

3.2. The boundary conditions at the interface

A main issue of the algorithms is updating the Robin data η_{f}^{k+1} and η_{p}^{k+1}, steps 2 and 4 of Algorithm S and step 2 of Algorithm P.

In [10, 12, 16], the following approach was considered, with $\theta = 1$,

$$\eta_{\mathrm{f}}^{k+1} = (1 - \theta)\eta_{\mathrm{f}}^{k} + \theta \left(\frac{\gamma_{\mathrm{f}}}{\gamma_{\mathrm{p}}} \eta_{\mathrm{p}}^{k} - \frac{\gamma_{\mathrm{p}} + \gamma_{\mathrm{f}}}{\gamma_{\mathrm{p}}} g \varphi_{\mathrm{p}}^{k+1} \right), \tag{27}$$

$$\eta_{\mathrm{p}}^{k+1} = (1 - \theta)\eta_{\mathrm{p}}^{k} + \theta \left(-\eta_{\mathrm{f}}^{\tilde{k}} + (\gamma_{\mathrm{p}} + \gamma_{\mathrm{f}}) \mathbf{u}_{\mathrm{f}}^{k+1} \cdot \mathbf{n}_{\mathrm{f}} \right). \tag{28}$$

This updating strategy is a damped version of applying the second and fourth line in (26), i.e., it originates from a Robin–Robin formulation for the Neumann–Neumann coupled problem. Using conforming finite element spaces, then $\varphi_{\mathrm{p}}^{k+1}$ and $\mathbf{u}_{\mathrm{f}}^{k+1}$ are continuous functions. Thus, if η_{f}^{0} and η_{p}^{0} are also continuous, then the updating strategy (27), (28) gives also continuous Robin boundary data at the interface. For this reason, it will be called C-RR (continuous Robin–Robin).

For $\theta = 1$, Algorithm S with the updating strategy C-RR is the Robin–Robin method that was analyzed in [12]. This analysis covers the convergence of the method in the setting of infinite dimensional spaces, where the Stokes–Darcy problem with the interface conditions (6), (7), and (10) was considered. The updating strategy C-RR (with $\theta = 1$) with Algorithm P was proposed and analyzed in [16]. In this paper, the Stokes–Darcy problem with the coupling conditions (6), (7), and the Beavers–Joseph–Saffman condition (9) was studied. Although both approaches are rather similar, the corresponding algorithms rely on completely different choices of the Robin parameters: $\gamma_{\mathrm{f}} > \gamma_{\mathrm{p}}$ for small ν and K in [12] and $\gamma_{\mathrm{f}} < \gamma_{\mathrm{p}}$ for unitary ν and K in [16]. In both cases, it was reported that the opposite choice would not lead to an efficient strategy. On the one hand, both papers [12] and [16] study different regimes of the coefficients of the Stokes–Darcy problem, but on the other hand, a dependence of the Robin parameters on these coefficients is not considered. Altogether, it remains still unclear how to choose the Robin–Robin parameters for given ν and K in general situations.

A different updating strategy consists in applying

$$\eta_{\mathrm{f}}^{k+1} = (1-\theta)\eta_{\mathrm{f}}^k + \theta\big(-g\varphi_{\mathrm{p}}^{k+1} - \gamma_{\mathrm{f}}\mathbb{K}\nabla\varphi_{\mathrm{p}}^{k+1}\cdot\mathbf{n}_{\mathrm{f}}\big), \tag{29}$$

$$\eta_{\mathrm{p}}^{k+1} = (1-\theta)\eta_{\mathrm{p}}^k + \theta\big(\gamma_{\mathrm{p}}\mathbf{u}_{\mathrm{f}}^{k+1}\cdot\mathbf{n}_{\mathrm{f}} - \mathbf{n}_{\mathrm{f}}\cdot\mathbb{T}(\mathbf{u}_{\mathrm{f}}^{k+1}, p_{\mathrm{f}}^{k+1})\cdot\mathbf{n}_{\mathrm{f}}\big). \tag{30}$$

This strategy corresponds to using the second and fourth row of (24), together with a damping, i. e., it comes from a Robin–Robin formulation. Note that for continuous finite element spaces, $\nabla\varphi_{\mathrm{p}}^{k+1}$ and $\mathbb{T}(\mathbf{u}_{\mathrm{f}}^{k+1}, p_{\mathrm{f}}^{k+1})$ are in general discontinuous functions, such that (29) and (30) lead to discontinuous Robin boundary data. Thus, this strategy will be called D-RR (discontinuous Robin–Robin).

In the literature, we could find the use of the D-RR updating strategy only in [29], within Algorithm S.

Remark 3.1 (Possible variations)
In Algorithm S one could as well solve a Stokes problem first and then a Darcy problem in every iteration step. Furthermore the damping factor θ could be different for the update of the two interface variables η_{f}^{k+1} and η_{p}^{k+1}. Another modification of the D-RR updating strategy could be to use the solution from the previous iteration step instead of the previous interface variable, i. e.,

$$\eta_{\mathrm{f}}^{k+1} = (1-\theta)\big(-g\varphi_{\mathrm{p}}^k - \gamma_{\mathrm{f}}\mathbb{K}\nabla\varphi_{\mathrm{p}}^k\cdot\mathbf{n}_{\mathrm{f}}\big) + \theta\big(-g\varphi_{\mathrm{p}}^{k+1} - \gamma_{\mathrm{f}}\mathbb{K}\nabla\varphi_{\mathrm{p}}^{k+1}\cdot\mathbf{n}_{\mathrm{f}}\big),$$

$$\eta_{\mathrm{p}}^{k+1} = (1-\theta)\big(\gamma_{\mathrm{p}}\mathbf{u}_{\mathrm{f}}^k\cdot\mathbf{n}_{\mathrm{f}} - \mathbf{n}_{\mathrm{f}}\cdot\mathbb{T}(\mathbf{u}_{\mathrm{f}}^k, p_{\mathrm{f}}^k)\cdot\mathbf{n}_{\mathrm{f}}\big) + \theta\big(\gamma_{\mathrm{p}}\mathbf{u}_{\mathrm{f}}^{k+1}\cdot\mathbf{n}_{\mathrm{f}} - \mathbf{n}_{\mathrm{f}}\cdot\mathbb{T}(\mathbf{u}_{\mathrm{f}}^{k+1}, p_{\mathrm{f}}^{k+1})\cdot\mathbf{n}_{\mathrm{f}}\big).$$

In our experience so far, none of the proposed variations yields a qualitative difference to the results presented in Section 4.

3.3. Implementation aspects

The matrices corresponding to the Darcy and the Stokes problem with Robin boundary conditions do not change during the iterative processes in both Algorithms S and P. Therefore, one assembly prior to the iteration suffices and a factorization can be computed. Furthermore, the interface contribution $\langle\eta_{\mathrm{f}}^{k+1}, \mathbf{v}\cdot\mathbf{n}\rangle_{\Gamma_{\mathrm{I}}}$ (corresponding to $\mathcal{E}_{\mathrm{f}}$ in (24) and (25)), which is added to the right-hand side of the Stokes system, is linear in η_{f} and can be computed by a matrix-vector multiplication. Similar ideas apply to the update of the right-hand side in the Darcy problem, i. e., to the operator $\mathcal{E}_{\mathrm{p}}$, and to the restriction operators $\mathcal{R}_{\mathrm{p}}$, $\mathcal{R}_{\mathrm{f}}$, $\mathcal{R}_{\mathrm{p,rob}}$, $\mathcal{R}_{\mathrm{f,rob}}$ in (24) and (25), respectively. Hence, no further assembling is needed during the iteration.

The simplified condition (10) is implemented weakly, penalizing the tangential component of the velocity on the interface by a Nitsche technique [30, 31], rather than imposing it directly in the velocity function spaces. It is assumed that the Stokes subdomain is triangulated with a regular finite element mesh which induces a partition on the (conformal) interface Γ_{I}. Denoting by h_E the diameter of a face (edge) $E \subset \Gamma_{\mathrm{I}}$, then for imposing the interface condition (10), the following term is added to the formulation

$$-\sum_{i=1}^{d-1}\langle\boldsymbol{\tau}_i\cdot\mathbb{T}(\mathbf{u}_{\mathrm{f}}, p_{\mathrm{f}})\cdot\mathbf{n}_{\mathrm{f}}, \mathbf{v}\cdot\boldsymbol{\tau}_i\rangle_{\Gamma_{\mathrm{I}}} + \sum_{i=1}^{d-1}\sum_{E\in\Gamma_{\mathrm{I}}}\frac{\gamma}{h_E}\langle\mathbf{u}_{\mathrm{f}}\cdot\boldsymbol{\tau}_i, \mathbf{v}\cdot\boldsymbol{\tau}_i\rangle_E,$$

where $\gamma > 0$ is a constant penalty parameter, whose value depends in general on the particular problem [30]. We used $\gamma = 10$ in all simulations. The first term resulting from integration by parts is not replaced but it enters the matrix.

3.4. Stopping criteria

Standard stopping criteria, e.g., the ones used in [10, 12], depend on the absolute or relative differences between successive iterates, computed on pressure or velocity solution vectors or

on interface variables, i.e., based on terms of the form

$$\left\| s_h^{k+1} - s_h^k \right\|_{\ell^2} \quad \text{or} \quad \frac{\left\| s_h^{k+1} - s_h^k \right\|_{\ell^2}}{\left\| s_h^k \right\|_{\ell^2}},$$

where s_h^k stands for $\mathbf{u}_{\mathrm{f},h}^k$, $p_{\mathrm{f},h}^k$, $\varphi_{\mathrm{p},h}^k$, $\eta_{\mathrm{p},h}^k$, or $\eta_{\mathrm{f},h}^k$. In [10, 12], the relative increment of the discrete normal velocity on the interface $\mathbf{u}_{\mathrm{f},h} \cdot \mathbf{n}_{\mathrm{f}}|_{\Gamma_{\mathrm{I}}}$ was used. Another possibility consists in checking the accuracy of the coupling conditions (6) and (7), i.e., monitoring the term

$$e^k := \left\| \mathbf{u}_{\mathrm{f},h}^k + \mathbb{K}\nabla\varphi_{\mathrm{p},h}^k \cdot \mathbf{n}_{\mathrm{f}} \right\|_{L^2(\Gamma_{\mathrm{I}})}^2 + \left\| \mathbf{n}_{\mathrm{f}} \cdot \mathbb{T}(\mathbf{u}_{\mathrm{f},h}^k, p_{\mathrm{f},h}^k) \cdot \mathbf{n}_{\mathrm{f}} + g\varphi_{\mathrm{p},h}^k \right\|_{L^2(\Gamma_{\mathrm{I}})}^2.$$

However, these quantities depend on the considered finite element spaces and, in general, they might not vanish even for the exact solution of the discrete coupled linear system. On the other hand, the relative difference

$$E_k := \frac{e^k - e^{k+1}}{e^k} = 1 - \frac{e^{k+1}}{e^k}$$

provides a measure of the progress made in the iteration. All these criteria can be used on their own or in some (linear) combination. However these stopping criteria only measure the progress of the iteration but not the quality of the solution, i.e., they are not able to detect whether the computed iterate is indeed close to the solution of the discrete problem or if the iteration sticks at an early stage. Therefore, we considered a further stopping criterion based on the residual of the (discrete versions of the) equations (17) or (23), i.e.,

$$R_k := \left\| \begin{pmatrix} \mathcal{D}_h & \mathcal{C}_h \\ \mathcal{C}_h^\top & \mathcal{S}_h \end{pmatrix} \begin{pmatrix} \varphi_{\mathrm{p},h}^{k+1} \\ s_{\mathrm{f},h}^{k+1} \end{pmatrix} - \begin{pmatrix} \mathcal{F}_{\mathrm{f},h} \\ \mathcal{F}_{\mathrm{p},h} \end{pmatrix} \right\|_{\ell^2}.$$

If not stated otherwise, in the simulations presented in Section 4, the iterative procedure has been stopped when the following conditions were satisfied

$$R_k < \mathrm{eps} \qquad \text{and} \qquad \frac{\left\| \mathbf{u}_{\mathrm{f},h}^{k+1} - \mathbf{u}_{\mathrm{f},h}^k \right\|_{\ell^2}}{\left\| \mathbf{u}_{\mathrm{f},h}^k \right\|_{\ell^2}} + \frac{\left\| p_{\mathrm{f},h}^{k+1} - p_{\mathrm{f},h}^k \right\|_{\ell^2}}{\left\| p_{\mathrm{f},h}^k \right\|_{\ell^2}} + \frac{\left\| \varphi_{\mathrm{p},h}^{k+1} - \varphi_{\mathrm{p},h}^k \right\|_{\ell^2}}{\left\| \varphi_{\mathrm{p},h}^k \right\|_{\ell^2}} < \mathrm{eps}, \quad (31)$$

for a prescribed threshold eps. In the second condition, we omitted the denominator whenever it was smaller than one.

4. COMPUTATIONAL RESULTS

The goal of the numerical studies consists in assessing Algorithms S and P in combination with the updating strategies C-RR and D-RR with respect to their efficiency. Since in all methods, the numerical costs per iteration are very similar, the efficiency will be measured in terms of the number of iterations for reaching convergence. Because of our motivation to study applications in computational geosciences, the algorithms will be assessed especially for physical parameters which are relevant in this context.

For all numerical experiments, the Taylor–Hood P_2/P_1 pair of finite element spaces was used in the Stokes subdomain, while P_2 elements have been used for the piezometric head. This choice of spaces is the same as, e.g., in [10, 12, 16]. The Robin–Robin updating strategies were applied with $\theta = 1$. All simulations were performed with the code MooNMD [26]. The linear systems of equations were solved with the sparse direct solver UMFPACK [32].

To verify the implementation, the solver was benchmarked considering a solution belonging to the finite element spaces. In these studies, the final errors for $\nu = 1$ and $\mathbb{K} = \mathbb{I}$ were of the order of the machine accuracy, but they increased with ν^{-1} and $\mathbb{K}^{-1}$. This observation reflects

the fact that, for small ν and $\mathbb{K}$, the condition numbers of the finite element linear systems increase.

As already mentioned above, a motivation for the present study is the unclear situation concerning the choice of the Robin parameters γ_f and γ_p. To address this question, we first validated our implementation against two examples taken from [10, 12, 16], to reproduce the published results using the algorithms considered in the respective paper. In addition, all other algorithms were also assessed for these examples. Finally, we studied an example related to a geoscientific application [33, 34].

4.1. Example 1

This example was used in [16] to illustrate the behavior of Algorithm P with the C-RR updating strategy for the viscosity $\nu = 1$ and the hydraulic conductivity $\mathbb{K} = \mathbb{I}$.

Let $\Omega_p = (0, \pi) \times (-1, 0)$, $\Omega_f = (0, \pi) \times (0, 1)$, and $\Gamma_I = (0, \pi) \times \{0\}$. The hydraulic conductivity has the form $\mathbb{K} = K\mathbb{I}$, and the solution of the coupled problem (1), (2), (5) is given by

$$\mathbf{u}_f(x, y) = \begin{pmatrix} v'(y) \cos(x) \\ v(y) \sin(x) \end{pmatrix}, \quad p_f(x, y) = 0, \quad \varphi_p(x, y) = e^y \sin(x),$$

where

$$v(y) = -K - \frac{gy}{2\nu} + \left(-\frac{\alpha g}{4\nu^2} + \frac{K}{2} \right) y^2.$$

On the outer boundaries, i.e., $\Gamma_{f,e} = \partial\Omega_f \setminus \Gamma_I$ and $\Gamma_{p,e} = \partial\Omega_p \setminus \Gamma_I$, essential boundary conditions were prescribed. This example considers the Beavers–Joseph–Saffman condition, i.e., the coupling conditions at the interface are given by (6), (7), and (9). Numerical simulations were performed on meshes obtained by uniformly red refining an initial coarse grid (level 0) consisting of eight triangles, see Figure 2. Note that no information about the mesh is available in [16], such that our setup might be different in this respect. The initial iterate was always set to be zero. The iterative algorithm was stopped according to the criterion (31) with a tolerance $\text{eps} = 10^{-10}$. The use of this stopping criterion is another difference to [16].
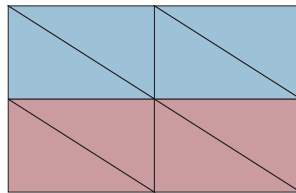

Figure 2. Example 1: initial grid (level 0) with Ω_f in blue (top) and Ω_p in red (bottom).

Since the main goal of this first example is the validation of our results against the results from [16], only the case $\nu = 1$ and $\mathbb{K} = \mathbb{I}$ will be considered. Figure 3 shows the evolution of the relative discrete errors of the iterates of the Stokes velocity, for different choices of the Robin parameters. In all cases, the curves are in agreement with the results reported in [16, Fig. 6.1]. Details concerning the needed iterations are provided in Table I. For the updating strategy D-RR, Algorithm S converged faster than Algorithm P. Moreover, for all methods, the number of iterations is independent of the level. As stated also in [16], one can see in Figure 3 a very fast convergence if $\gamma_f < \gamma_p$, a slow convergence if $\gamma_f = \gamma_p$, and divergence in the case $\gamma_f > \gamma_p$. The speed of convergence depends essentially on the ratio γ_f/γ_p. In this example, the smallest number of iterations were needed for $\gamma_p = 1$. We could observe the same convergence behavior for the Stokes pressure and the piezometric head.

In summary, the results from [16] could be reproduced very well.

Updating strategy	Algorithm	Level 1	Level 2	Level 3	Level 4
C-RR	Algorithm P	19	19	19	20
C-RR	Algorithm S	19	19	19	20
D-RR	Algorithm P	34	36	36	36
D-RR	Algorithm S	19	19	19	20

Table I. Example 1: Number of iterations for $\gamma_\mathrm{p} = 1$ and $\gamma_\mathrm{f} = \gamma_\mathrm{p}/3$.

4.2. Example 2

This example was used in [10, 12] for assessing Algorithm S with the C-RR updating strategy for different values of the kinematic viscosity ν and the hydraulic conductivity K.

Let $\Omega_\mathrm{p} = (0, 1)^2$ and $\Omega_\mathrm{f} = (0, 1) \times (1, 2)$, with the interface $\Gamma_\mathrm{I} = \partial\Omega_\mathrm{p} \cap \partial\Omega_\mathrm{f} = (0, 1) \times \{1\}$, the hydraulic conductivity of the form $\mathbb{K} = K\mathbb{I}$, and the solution given by

$$
\begin{aligned}
\mathbf{u}_s(x, y) &= \begin{pmatrix} y^2 - 2y + 1 \\ x^2 - x \end{pmatrix}, \\
p_\mathrm{f}(x, y) &= 2\nu(x + y - 1) + \frac{g}{3K}, \\
\varphi_\mathrm{p}(x, y) &= \frac{1}{K}\left(x(1 - x)(y - 1) + \frac{y^3}{3} - y^2 + y\right) + \frac{2\nu}{g}x.
\end{aligned}
\tag{32}
$$

Dirichlet boundary conditions were imposed on $\partial\Omega_\mathrm{f} \setminus \Gamma_\mathrm{I}$ and on the bottom boundary $(0, 1) \times \{0\}$. On the remaining parts, Neumann boundary conditions were prescribed. In this example, the simplified Beavers–Joseph–Saffman condition (6), (7), and (10) is considered. We used unstructured grids with 98 (mesh 1), 470 (mesh 2), 1914 (mesh 3) and 8216 (mesh 4) cells with a total of 406 (mesh 1), 1690 (mesh 2), 6553 (mesh 3) and 27402 (mesh 4) degrees of freedom. The initial iterate was always chosen to be zero.

Using values for the parameters ν and K relevant for geoscientific applications, which are typically very small, the pressure and the piezometric head in (32) consist of two parts. A very small contribution scaled with ν and a very large part due to the scaling with K^{-1}. This second part leads to values of p_f and φ_p which are unrealistic in applications. In this respect, this example has some deficiencies.

To reproduce the results from [10, 12], we first used as stopping criterion only

$$
\frac{\left\|\mathbf{u}_\mathrm{f}^{k+1} - \mathbf{u}_\mathrm{f}^k\right\|}{\left\|\mathbf{u}_\mathrm{f}^k\right\|} < 10^{-6},
\tag{33}
$$

similarly as it has been applied in [10, 12], where the relative increment of the discrete normal velocity on the interface and a somewhat smaller tolerance were used. Note that $\mathbf{u}_\mathrm{f}$ is the only part of the solution that does not scale with K^{-1}. Because of the large condition number of the linear system of equations for small ν and K, which was already mentioned above, one generally has to relax the tolerances of stopping criteria in this case compared with the case $\nu = 1$, $K = 1$.

Table II reports the results with Robin parameters $\gamma_\mathrm{p} = 1$, $\gamma_\mathrm{f} = \frac{\gamma_\mathrm{p}}{3}$, which was the most efficient choice in Example 1, in combination with the stopping criterion (33). Clearly, all algorithms failed for those parameters in the case of small ν and small K.

Indeed, following [10, 12], one would expect efficient simulations for a different choice of the Robin parameters, namely $\gamma_\mathrm{p} = 0.1$, $\gamma_\mathrm{f} = 3\gamma_\mathrm{p}$. In this case, one obtains the results presented in Table III. One can see that the algorithms with the updating strategy D-RR converged for all choices of physical parameters. We observed a similar behavior of the algorithms with the D-RR updating strategy also for $\gamma_\mathrm{f} = 3\gamma_\mathrm{p}$ with $\gamma_\mathrm{p} \in \{1, 10, 50, 100, 200\}$. The results are similar

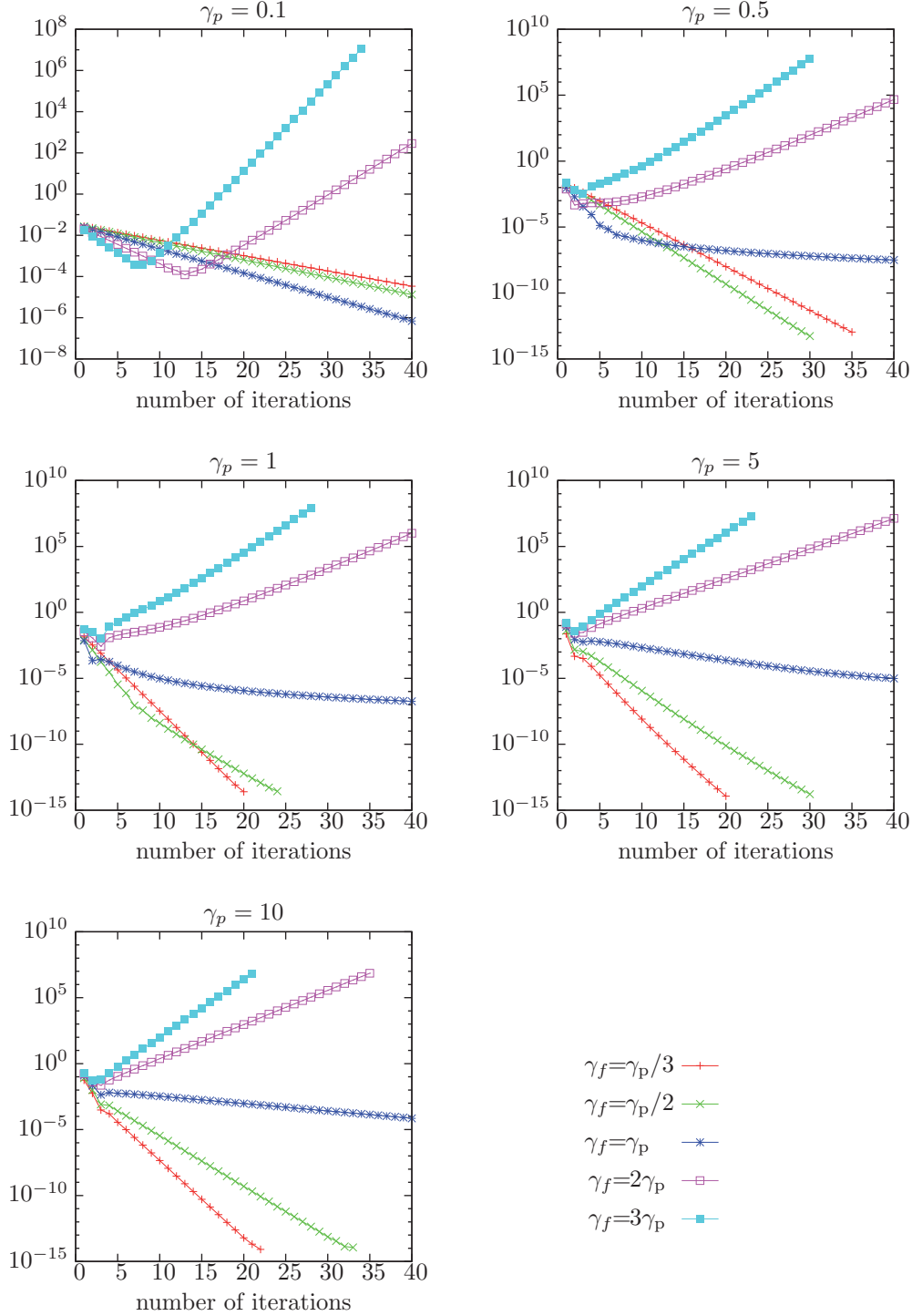Relative discrete errors for the Stokes velocity

Figure 3. Example 1: Relative discrete errors $\frac{\left\|\mathbf{u}_{\mathrm{f},h}^{k+1}-\mathbf{u}_{\mathrm{f},h}\right\|_{\ell^2}}{\|\mathbf{u}_{\mathrm{f},h}\|_{\ell^2}}$ of Algorithm S with $\nu = 1$ and $K = 1$, for different values of γ_{p} and γ_{f} on refinement level 4.

Updating strategy	Algorithm	ν	K	mesh 1	mesh 2	mesh 3	mesh 4
C-RR	Algorithm P	1	1	7	7	7	7
		10	10^{-1}	25	25	25	25
		10^{-2}	10^{-2}	—	—	—	—
	Algorithm S	1	1	7	7	7	7
		10	10^{-1}	11	11	11	11
		10^{-2}	10^{-2}	—	—	—	—
D-RR	Algorithm P	1	1	9	9	11	11
		10	10^{-1}	18	20	20	20
		10^{-2}	10^{-2}	+++	+++	+++	+++
	Algorithm S	1	1	5	6	7	7
		10	10^{-1}	10	11	11	11
		10^{-2}	10^{-2}	—	—	—	—
all	both	10^{-3}	10^{-2}	—	—	—	—
		10^{-4}	10^{-3}	—	—	—	—
		10^{-6}	10^{-4}	—	—	—	—
		10^{-6}	10^{-7}	—	—	—	—

Table II. Example 2 Number of iterations for $\gamma_{\mathrm{p}} = 1$ and $\gamma_{\mathrm{f}} = \gamma_{\mathrm{p}}/3$, stopping criterion (33), "+++" means did not converge within 100 iterations and "—" means diverged.

type	algorithm	ν	K	mesh 1	mesh 2	mesh 3	mesh 4
C-RR	Algorithm P	10^{-4}	10^{-3}	—	—	—	—
		10^{-6}	10^{-4}	—	—	—	—
		10^{-6}	10^{-7}	—	—	—	—
	Algorithm S	10^{-4}	10^{-3}	207	51	27	21
		10^{-6}	10^{-4}	274	12	12	12
		10^{-6}	10^{-7}	12	12	12	12
D-RR	Algorithm P	10^{-4}	10^{-3}	15	15	17	17
		10^{-6}	10^{-4}	7	9	9	9
		10^{-6}	10^{-7}	7	9	9	9
	Algorithm S	10^{-4}	10^{-3}	11	11	11	11
		10^{-6}	10^{-4}	12	12	12	12
		10^{-6}	10^{-7}	12	12	12	12

Table III. Example 2: Number of iterations for the stopping criterion (33), $\gamma_{\mathrm{p}} = 0.1$ and $\gamma_{\mathrm{f}} = 0.3$, "—" means diverged.

to those reported in [10, 12] for the updating strategy C-RR. In our simulations, however, the C-RR updating strategy was less successful for all studied choices of the Robin parameters and we could not reproduce the results from [10, 12]. Consulting the Ph.D. thesis [29], one gets the impression that in [10, 12] the C-RR updating strategy is presented and analyzed but the numerical studies in these papers were performed with the D-RR updating strategy.

In Table III, one can see that Algorithm P was (for the D-RR updating strategy) more efficient than Algorithm S for very small values of the physical coefficients. For both algorithms, the number of iterations is independent of the mesh.

Next, the convergence properties of the algorithms using the harder stopping criterion (31), also with eps = 10^{-6}, were investigated. One can observe in Figure 4 that for $\gamma_{\mathrm{p}} = 0.1$, $\gamma_{\mathrm{f}} = 3\gamma_{\mathrm{p}}$

(we obtained similar results for $\gamma_p \in \{\frac{1}{30}, \frac{1}{3}, 1\}$) even if the criterion (33) is satisfied, the residual of the complete coupled problem is far from being small. Figure 4 shows also that relative changes of the pressure and the piezometric head are still large. For further comparisons, we computed the solution of the monolithic discrete Stokes–Darcy problem by applying a direct solver to the coupled finite element problem (an approach which is not feasible in many applications). Then, one can see that the iterates for the pressure and the piezometric head still differ considerably from the discrete solution. These observations confirm that the stopping criterion (33) is not sufficient to assess the properties of the iterative algorithms, and the number of iterations given in Table III might provide a wrong impression of their efficiency.

Further numerical studies revealed that a considerable speed-up of the algorithms with the D-RR updating strategy could be achieved by increasing the Robin parameters, thereby keeping the relation $\gamma_f = 3\gamma_p$, see Figure 5 and Table IV. Similar results were obtained for $\gamma_p \in \{50, 200\}$. We think that the slow convergence in the case $K = 10^{-7}$ is due to the unrealistic large values for the pressure and the hydraulic head. One can see in Table IV that Algorithm S performed better than Algorithm P. The number of iterations is independent of the mesh.
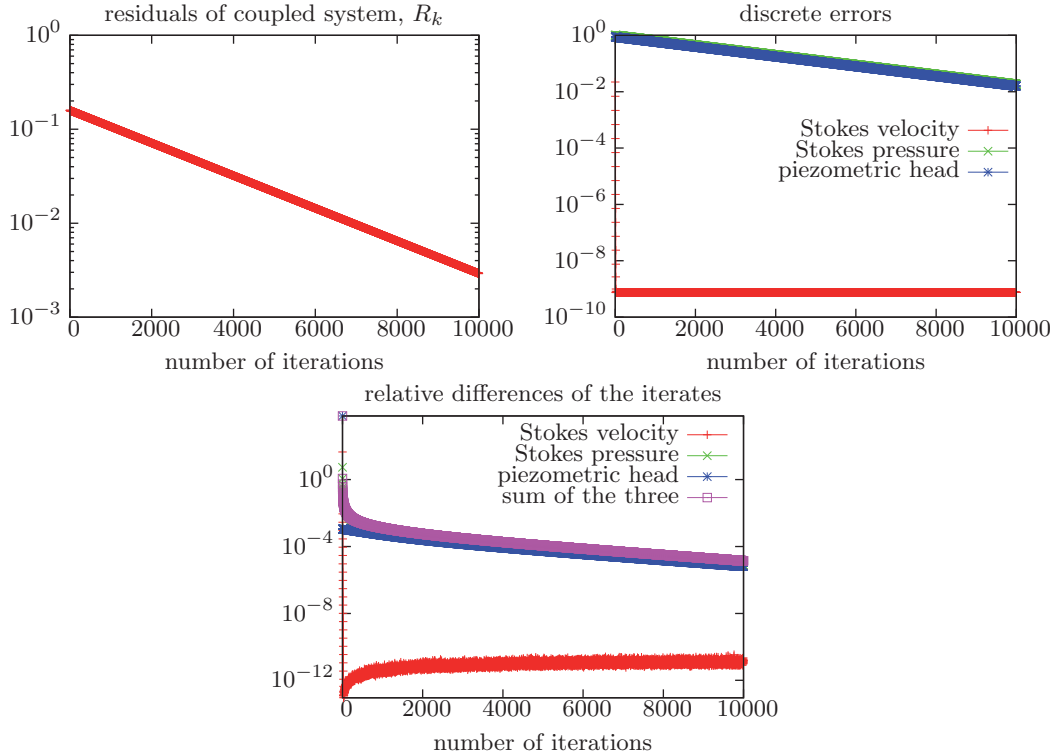

Figure 4. Example 2: Evolution of the residual, discrete errors, and relative differences for Algorithm S, mesh 4, using the D-RR updating strategy and $\gamma_p = 0.1$, $\gamma_f = 3\gamma_p$, $\nu = 10^{-4}$, and $K = 10^{-3}$.

In summary, despite the shortcomings of the used example, it was clarified that for the case of small viscosity and small hydraulic conductivity, the use of the D-RR updating strategy and the choice $\gamma_f > \gamma_p$, e.g., $\gamma_f = 3\gamma_p$, of the Robin parameters are important to obtain an efficient subdomain iteration.

4.3. Example 3: Water flow over a porous river bed

As a final example, a model of a unidirectional steady water flow over a porous bed is considered, separated by a non-straight interface. In the context of computational geosciences,
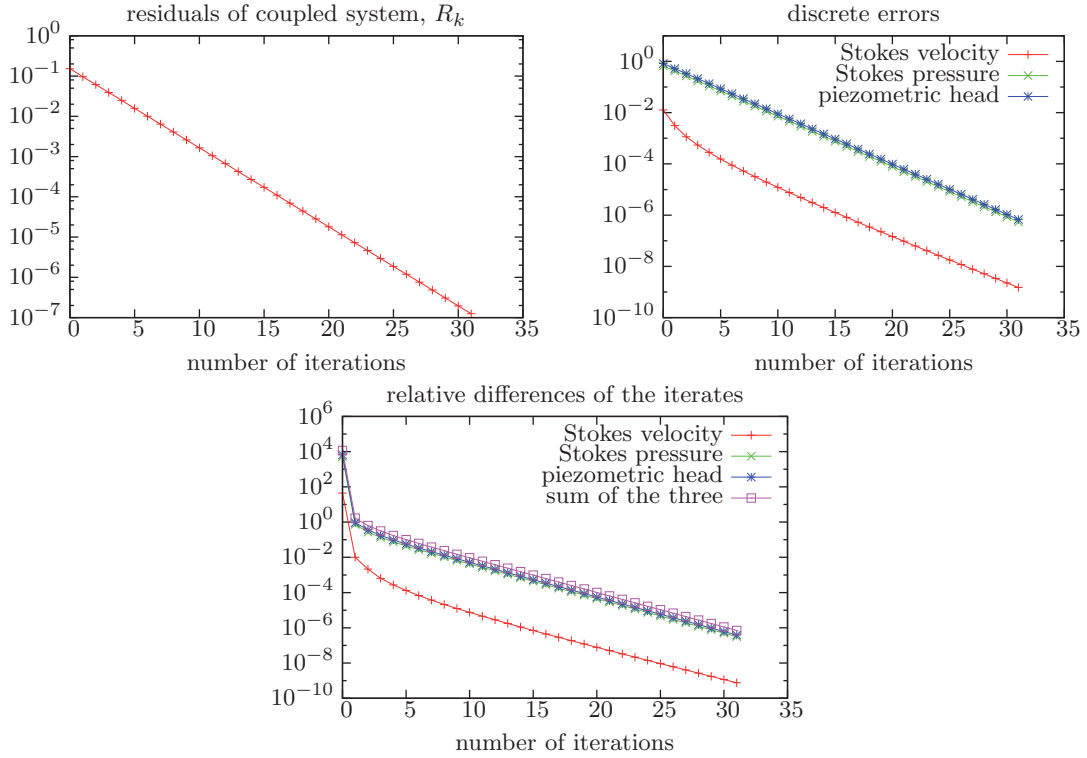
Figure 5. Example 2: Evolution of the residual, discrete errors, and relative differences versus the number of iterations for Algorithm S, mesh 4, using the D-RR updating strategy and $\gamma_p = 100$, $\gamma_f = 3\gamma_p$, $\nu = 10^{-4}$, and $K = 10^{-3}$.

type	algorithm	ν	K	mesh 1	mesh 2	mesh 3	mesh 4
C-RR	Algorithm P	10^{-4}	10^{-3}	—	—	—	—
		10^{-6}	10^{-4}	—	—	—	—
		10^{-6}	10^{-7}	—	—	—	—
	Algorithm S	10^{-4}	10^{-3}	—	—	—	—
		10^{-6}	10^{-4}	432	422	413	—
		10^{-6}	10^{-7}	+++	+++	+++	+++
D-RR	Algorithm P	10^{-4}	10^{-3}	76	74	72	71
		10^{-6}	10^{-4}	841	823	805	787
		10^{-6}	10^{-7}	+++	+++	+++	+++
	Algorithm S	10^{-4}	10^{-3}	32	32	32	32
		10^{-6}	10^{-4}	326	316	307	298
		10^{-6}	10^{-7}	+++	+++	+++	+++

Table IV. Example 2: Number of iterations for the stopping criterion (31), $\gamma_p = 100$ and $\gamma_f = 300$, "+++" means did not converge within 1000 iterations, "—" means diverged.

this model has been proposed for the study of the hydrodynamic interactions between the water flow and the underlying river bed [33, 34].

In order to simulate the water flow over two triangular dunes, consider a rectangular domain

$$\Omega = [0, 2L] \times [0, H_f + H_p],$$

where H_f and H_p denote the heights of the water flow domain and the porous river bed at $x \in \{0, L, 2L\}$. The interface, representing the dune, is composed of two triangles, whose highest points are located at $x \in \{l_D, L + l_D\}$, while the maximum height of the dunes, with respect to the entrance porous bed, is denoted by h_D, see Figure 6.
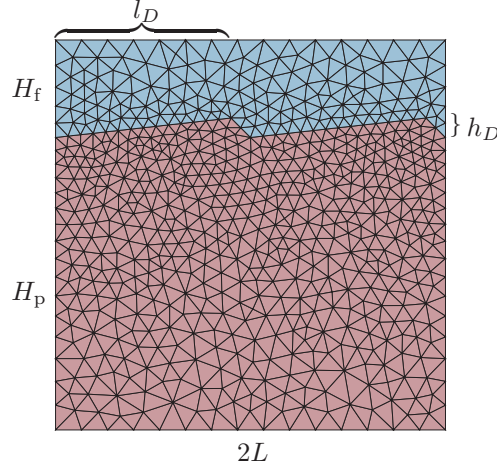

Figure 6. Computational domain for the water flow over a porous river bed model, mesh 1.

The boundary conditions and the values of the physical parameters have been chosen as in the numerical simulations presented in [33, 34]. In particular, the lower boundary is considered impermeable (no flow boundary condition), while no-slip conditions are imposed at the upper boundary. At inlet and outlet boundaries, the following inhomogeneous periodic boundary conditions for Stokes and Darcy problems have been imposed:

$$\mathbf{u}_{\mathrm{inlet}} = \mathbf{u}_{\mathrm{outlet}},$$
$$T(\mathbf{u}_{\mathrm{inlet}}, p_{\mathrm{inlet}}) \cdot \mathbf{n}_{\mathrm{f}} = T(\mathbf{u}_{\mathrm{outlet}}, p_{\mathrm{outlet}}) \cdot \mathbf{n}_{\mathrm{f}} + p_0,$$
$$\varphi_{\mathrm{inlet}} = \varphi_{\mathrm{outlet}} + p_0.$$

Note that the pressure is unique only up to an additive constant in this example. We fixed this constant by forcing one pressure node to be zero. Furthermore, the simulation parameters are

$$L = 1, \ H_{\mathrm{f}} = 0.5, \ H_{\mathrm{p}} = 1.5,$$
$$l_D = 0.9, \ h_D = 0.1,$$
$$p_0 = 10^{-3}, \ \mathbf{f}_{\mathrm{f}} = 0, \ f_{\mathrm{p}} = 0.$$

Figure 7 depicts the numerical solution for $\nu = 10^{-6}$ and $K = 10^{-7}$. The prescribed pressure drop p_0 induces a flow from left to right, which partially penetrates the porous bed due to the inclination of the interface. However, the impact of the water flow onto the porous media (and vice versa) remains local, i.e., the flow remains unperturbed and unidirectional away from the interface. Note the pressure drop arising behind the dunes, which locally causes a flow in the opposite direction underneath the dunes.

For assessing the performance of the iterative algorithms, three different unstructured meshes were considered, see Figure 6 for an example and Table V for detailed information. From the results obtained in Example 2, it can be expected that one has to use the updating strategy D-RR. In fact, we could observe in this example that the subdomain iteration did not converge if the updating strategy C-RR was employed. The obtained results are presented in Tables VI and VII, where the threshold of the stopping criterion (31) was set to be eps $= 10^{-6}$. Different values of the Robin parameters γ_{f} and γ_{p} were chosen, always satisfying the same ratio as in Example 2 and in [10, 12]. One can see that both algorithms performed well on all meshes for the Robin parameters $\gamma_{\mathrm{p}} \in \{10, 100\}$ and $\gamma_{\mathrm{f}} = 3\gamma_{\mathrm{p}}$. The number of iterations for Algorithm S was in the most cases independent of the mesh. For some physical parameters, in particular for very small ν and K, Algorithm P converged faster than Algorithm S.
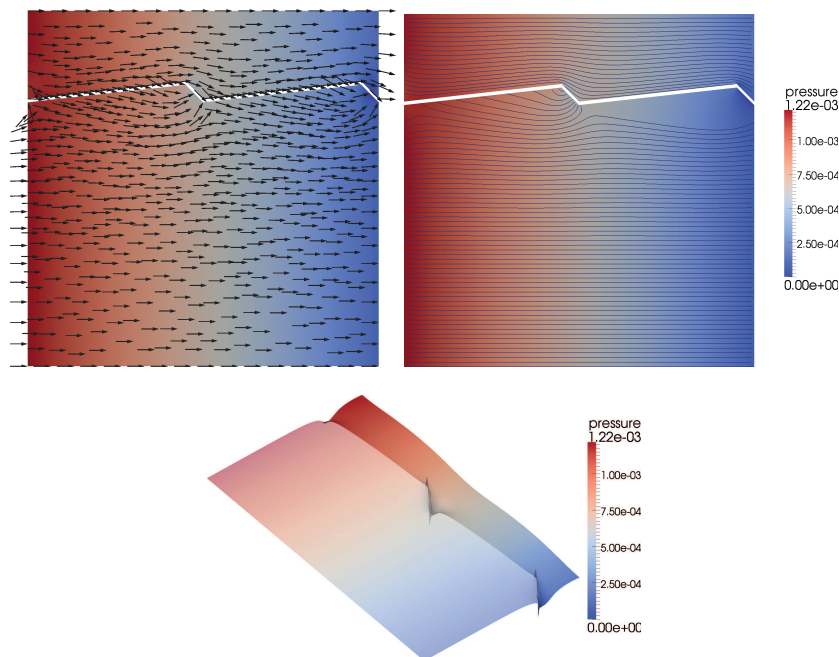
Figure 7. Example 3: Numerical solution for $\nu = 10^{-6}$ and $K = 10^{-7}$, showing the velocity field $\mathbf{u}_{\mathrm{f}}$ and $\nabla\varphi_{\mathrm{p}}$ (unscaled arrows, top left), the velocity streamlines (top right) and a pressure elevation plot which is semi-transparent in the Darcy subdomain (bottom). All three plots are colored according to the pressure field, scaled so that the minimum value is zero.

mesh	interface edges	cells		degrees of freedom	
		Stokes	Darcy	Stokes	Darcy
1	32	277	1 009	1 392	2 098
2	68	1 285	4 513	6 093	9 196
3	138	5 234	18 322	24 181	36 987

Table V. Example 3: Number of interface edges, Stokes and Darcy cells, and degrees of freedom for the three different meshes used.

5. SUMMARY AND OUTLOOK

This paper reviewed iterative subdomain methods for solving the Stokes–Darcy problem that use Robin boundary conditions at the interface. In particular, it was clarified that there are different updating strategies for the Robin boundary conditions. For coefficients in the Stokes–Darcy problem that are relevant for applications from geosciences, the use of the updating strategy D-RR, in combination with an appropriate choice of the Robin parameters, turned out to be crucial for designing an efficient numerical method. Concerning the Robin parameters, the choice $\gamma_{\mathrm{f}} = 3\gamma_{\mathrm{p}}$ resulted in efficient methods if γ_{p} was chosen appropriately, in the considered examples $\gamma_{\mathrm{p}} \in [10, 100]$. These values are considerably larger than those proposed so far in the literature. Finally, it was observed that the serial update of the interface conditions, Algorithm S, needed often less iterations than the parallel update, Algorithm P.

Altogether, the main goal of our studies was achieved: the identification of an efficient iterative subdomain method for the Stokes–Darcy problem with coefficients that are relevant in geosciences.

γ_{p}	γ_{f}	ν	K	mesh 1	mesh 2	mesh 3
1	3	10^{-4}	10^{-3}	+++	+++	+++
		10^{-6}	10^{-4}	+++	+++	+++
		10^{-6}	10^{-7}	+++	+++	+++
10	30	10^{-4}	10^{-3}	11	11	11
		10^{-6}	10^{-4}	12	12	13
		10^{-6}	10^{-7}	12	12	13
100	300	10^{-4}	10^{-3}	12	15	20
		10^{-6}	10^{-4}	12	12	13
		10^{-6}	10^{-7}	12	12	13

Table VI. Example 3: Number of iterations for the D-RR updating strategy and Algorithm S, "+++" means did not converge within 100 iterations.

γ_{p}	γ_{f}	ν	K	mesh 1	mesh 2	mesh 3
1	3	10^{-4}	10^{-3}	+++	+++	+++
		10^{-6}	10^{-4}	+++	+++	+++
		10^{-6}	10^{-7}	+++	+++	+++
10	30	10^{-4}	10^{-3}	15	15	17
		10^{-6}	10^{-4}	11	11	13
		10^{-6}	10^{-7}	9	7	9
100	300	10^{-4}	10^{-3}	17	27	39
		10^{-6}	10^{-4}	13	13	15
		10^{-6}	10^{-7}	3	5	7

Table VII. Example 3: Number of iterations for the D-RR updating strategy and Algorithm P, "+++" means did not converge within 100 iterations.

Further research include, e.g., studies of iterative subdomain methods for the Navier–Stokes–Darcy problem and a detailed investigation for the dual formulation of the Darcy problem, focusing on relevant situations for geoscientific applications. The numerical results presented in this paper showed that an appropriate choice of the Robin parameters γ_{f} and γ_{p} depends on the coefficients of the problem. Further comprehensive studies of this topic will be necessary to clarify the form of the dependence.

REFERENCES

1. Loula A, Rochinha F, Murad M. High-order gradient post-processing for second-order elliptic problems. *Comput. Meth Appl. Mech Engrg.* 1995; **125**:361–381.
2. Beavers G, Joseph D. Boundary conditions at a naturally permeable wall. *J. Fluid Mech.* 1967; **30**:197–207.
3. Angot P. On the well-posed coupling between free fluid and porous viscous flows. *Appl. Math. Lett.* 2011; **24**:803–810.
4. Cao Y, Gunzburger M, Hu X, Hua F, Wang X, Zhao W. Finite element approximations for Stokes-Darcy flow with Beavers-Joseph interface conditions. *SIAM J. Numer. Anal.* 2010; **47**(6):4239–4256.

5. Jaeger W, Mikelic A. On the interface boundary condition of Beavers, Joseph and Saffman. *SIAM J. Appl. Math.* 2000; **60**(4):1111–1127.
6. Saffman P. On the boundary condition at the interface of a porous medium. *Stud. Appl. Math.* 1971; **50**:93–101.
7. Jones I. Low Reynolds number flow past a porous spherical shell. *Math. Proc. Cambridge Philos. Soc.* 1973; **73**:231–238.
8. Levy T, Sanchez-Palencia E. On the boundary condition for fluid flow in porous media. *Int. J. Engng. Sci.* 1975; **13**:923–940.
9. Cao Y, Gunzburger M, Hua F, Wang X. Coupled Stokes-Darcy model with Beavers-Joseph interface boundary condition. *Commun. Math. Sci.* 2010; **8**(1):1–25.
10. Discacciati M, Quarteroni A. Navier-Stokes/Darcy coupling: modeling, analysis, and numerical approximation. *Rev. Mat. Complut.* 2009; **22**(2):315–426.
11. Discacciati M, Quarteroni A, Miglio E. Mathematical and numerical models for coupling surface and groundwater flows. *Appl. Numer. Math.* 2002; **43**:57–74.
12. Discacciati M, Quarteroni A, Valli A. Robin-Robin domain decomposition methods for the Stokes-Darcy coupling. *SIAM J. Numer. Anal.* 2007; **45**(3):1246–1268 (electronic).
13. Gatica GN, Oyarzua R, Sayas FJ. Analysis of fully-mixed finite element methods for the Stokes-Darcy coupled problem. *Math. Comp.* 2011; **80**:1911–1948.
14. Layton W, Schieweck F, Yotov I. Coupling fluid flow with porous media flow. *SIAM J. Numer. Anal.* 2003; **40**:2195–2218.
15. Riviére B, Yotov I. Locally conservative coupling of Stokes and Darcy flows. *SIAM J. Numer. Anal.* 2005; **42**:1955–1977.
16. Chen W, Gunzburger M, Hua F, Wang X. A parallel Robin-Robin domain decomposition method for the Stokes-Darcy system. *SIAM J. Numer. Anal.* 2011; **49**(3):1064–1084.
17. Zunino P, D'Angelo C. Robust numerical approximation of coupled Stokes' and Darcy's flows applied to vascular hemodynamics and biochemical transport. *ESAIM, Math. Model. Numer. Anal.* 2011; **45**(3):447–476.
18. Mardal K, Tai XC, Winther R. A robust finite element method for Darcy-Stokes flow. *SIAM J. Numer. Anal.* 2002; **40**:1605–1631.
19. Arbogast T, Brunson DS. A computational method for approximating a Darcy-Stokes system governing a vuggy porous medium. *Comput. Geosci.* 2007; **11**:207–218.
20. Burman E, Hansbo P. A unified stabilized method for Stokes' and Darcy's equations. *J. Comput. Appl. Math.* 2007; **198**(1):35–51.
21. Urquiza J, N'Dri D, Garon A, Delfour M. Coupling Stokes and Darcy equations. *Applied Numerical Mathematics* 2008; **58**(5):525 – 538.
22. Xie X, Xu J, Xue G. Uniformly-stable finite element methods for Darcy-Stokes-Brinkman models. *J. Comput. Math.* 2008; **26**:437–455.
23. Badia S, Codina R. Unified stabilized finite element formulations for the Stokes and the Darcy problems. *SIAM J. Numer. Anal.* 2009; **47**:1971–2000.
24. Mu M, Xu J. A two-grid method of a mixed Stokes–Darcy model for coupling fluid flow with porous media flow. *SIAM J. Numer. Anal.* 2007; **45**(5):1801–1813.
25. Cai M, Mu M. A multilevel decoupled method for a mixed Stokes–Darcy model. *J. Comput. Appl. Math.* 2012; **236**:2452–2465.
26. John V, Matthies G. MooNMD—a program package based on mapped finite element methods. *Comput. Vis. Sci.* 2004; **6**(2–3):163–169.
27. Discacciati M, Quarteroni A. Convergence analysis of a subdomain iterative method for the finite element approximation of the coupling of Stokes and Darcy equations. *Comput. Vis. Sci.* 2004; **6**(2-3):93–103, doi:10.1007/s00791-003-0113-0.
28. Juntunen M, Stenberg R. Nitsche's Method for General Boundary Conditions. *Math. Comp.* 2009; **78**(267):1353–1374.
29. Discacciati M. Domain Decomposition Methods for the Coupling of Surface and Groundwater Flows. PhD Thesis, École Polytechnique Fédérale de Lausanne 2004.
30. Nitsche J. Über ein Variationsprinzip zur Lösung von Dirichlet-Problemen bei Verwendung von Teilräumen, die keinen Randbedingungen unterworfen sind. *Abh. Math. Sem. Univ. Hamburg* 1971; **36**:9–15. Collection of articles dedicated to Lothar Collatz on his sixtieth birthday.
31. Freund J, Stenberg R. On weakly imposed boundary conditions for second order problems. *Proceedings of the Ninth Int. Conf. Finite Elements in Fluids* 1995; .
32. Davis TA. Algorithm 832: UMFPACK V4.3—an unsymmetric-pattern multifrontal method. *ACM Trans. Math. Software* 2004; **30**(2):196–199.
33. Cardenas M, Wilson J. Dunes, turbulent eddies, and interfacial exchange with permeable sediments. *Water Resour. Res.* 2007; **43**:08 412.
34. Cardenas M, Wilson J. Hydrodynamics of coupled ow above and below a sediment–water interface with triangular bedforms. *Adv. Water Resour.* 2007; **30**:301–313.